This is a preprint, the final version is subject to change, of the American Mineralogist (MSA)
Cite as Authors (Year) Title. American Mineralogist, in press.
DOI: https://doi.org/10.2138/am-2020-7154

Experimental study of the Pt and Pd antimonides and bismuthinides in Fe-Ni-Cu sulfide systems between 1100 and 700°C and applications to nature

(Revision 1)

Hassan M. Helmy[1,2] and Roman Botcharnikov[3]

[1] Department of Geology, Minia University, 61519-Minia, Egypt

[2] Steinmann Institute, Universität Bonn, Poppelsdorfer Schloss, 53115 - Bonn, Germany

[3] Institut für Geowissenschaften, Gutenberg Universität Mainz, Germany

Abstract

The stability of Pt and Pd antimonides and bismuthinides in the Sb- and Bi-bearing Fe-Ni-Cu sulfide systems are experimentally determined at temperatures between 1100 and 700°C in evacuated silica tubes. Both PtSb and PdSb are stable as immiscible liquids at temperatures above 1100 and 1000°C, respectively. The Fe-Ni-Cu-sulfide melt coexisting with immiscible antimonide melt can dissolve up to 3.8 wt.% Sb at 1100°C whereas monosulfide solid solution (mss) dissolves very low amounts of Sb over the entire 1100-700°C temperature range. The liquidus of Pt-antimonides and Pd-antimonides are above 980°C and 750°C, respectively. Bismuth does not form immiscible melt at 1100°C but may partially partition into a vapor phase at 1050°C. The Pt- and Pd-bismuthinides crystallize directly from immiscible bismuthinide melt only after crystallization of the sulfide melt into intermediate solid solution (iss). Insizwaite ($PtBi_2$) and froodite ($PdBi_2$) are stable at 780 and 700°C, respectively. At the last stage of evolution of Sb-bearing

magmatic Fe-Ni-Cu sulfide melts, Sb will form immiscible antimonide melt that will extract Pt and Pd from the sulfide melt. During cooling, Pt and Pd-antimonides will crystallize directly from the immiscible antimonide melt, and Pt-phases will form at higher temperatures relative to Pd-phases. Bismuth will partition into vapor phase and concentrate into a low-temperature melt In hydrothermal and porphyry systems which an scavenge precious metals. The Sb and Bi (like Te) will be highly incompatible at moderate degrees of mantle partial melting.

1. Introduction

Antimony (Sb) and bismuth (Bi) are semimetals that may influence the behavior of platinum-group elements (PGE) in nature. In base metal (Fe, Ni, Cu) sulfide systems, Sb and Bi behave largely as cations under both oxidized and reduced conditions. The partition coefficients of Sb and Bi between solid sulfide phase (monosulfide solid solution, mss) and the sulfide melt ($D^{\text{monosulfide solid solution/sulfide melt}}$) are less than 10^{-2} (Helmy et al., 2010). The two elements form stable intermetallic mineral phases with Pt and Pd in Cu-Ni sulfide ores, especially in those that have experienced extensive late-magmatic hydrothermal evolution or metamorphic overprint (e.g Helmy et al., 1995, Barkov et al., 2002; Spiridonov et al., 2015, O'Driscoll and González-Jiménez, 2016). Known Pt and Pd antimonides comprise stumpflite (PtSb), geversite ($PtSb_2$), genkinite (Pt_4Sb_3), subduryite (PdSb), naldrettite (Pd_2Sb), ungavaite (Pd_4Sb_3), mertiete ($Pd_{11}Sb_4$) and stibiopalladinte (Pd_5Sb_2). The Pt and Pd bismuthinides comprise insizwaite ($PtBi_2$), froodite ($PdBi_2$),

polarite (PdBi) and sobolevskite (PdBi). These minerals usually form micron-size grains along sulfide-silicate contacts, inclusions in base metal sulfides and silicates (Helmy et al., 1995; Barkov et al., 2002; Spiridonov et al., 2015, O'Driscoll and González-Jiménez, 2016, and many others). The Pt and Pd antimonides and bismuthinides are assumed to be formed by fractionation of a primary Cu-PGE-Sb-Bi-rich sulfide liquid (Graham et al., 2017) by direct crystallization from immiscible antimonide or bismuthinide melt (Holwell and McDonald, 2007).

In addition, Sb and Bi are important petrologic indicators in mantle processes (e.g. involvement of subduction components and crustal fluids, Scambelluri et al, 2014 and Jenner, 2017). For example, Noll et al (1996) noted that arc magmas are enriched in Sb relative to primitive mantle, which they attributed to supply from subducted slabs. Hattori et al (2002) attributed the low Sb (and As) contents in sulfides from mantle wedges to short residence of sulfides in the mantle wedge. They suggested that Sb (and As) are removed from the mantle during partial melting leading to low concentrations in sulfides in refractory mantle. The Sb and Bi enrichment in back arc basin basalts relative to MORB led Jenner (2017) to suggest that these elements are mobile and that their host phases (low temperature sulfides and sulfosalts) in the upper oceanic crust are unstable during subduction. Jenner (2017) stated that the unstable host phases of Sb and Bi release these elements leading to their mobility during subduction. There is also strong evidence that Sb can be added to magmas via contamination, usually along with As. For example, McDonald (2008) and Hutchinson and Kinnairid (2005) attributed the Sb-As

enrichment of magmas at Lavatrafo, Madagascar and in the Turfspruit sector of the Platreef to contamination by As-rich shales.

Despite the petrologic significance of Sb and Bi and their strong role in controlling the behavior of Pt and Pd in nature, their behavior in magmatic sulfide systems is poorly known. It is important, therefore, to know how Sb and Bi behave in magmatic sulfide systems to understand their behavior during subduction and contamination processes and in the formation of unusually Au-Ag-Pd rich porphyry deposits.. In addition, determining the sequence of crystallization and thermal stabilities of Pt and Pd antimonides and bismuthinides in magmatic sulfide systems is important in ore geology. In order to investigate this we have equilibrated Pt and Pd-antimonides and bismuthinides and $(Fe, Ni, Cu)_{1-x}S$ sulfides over a temperature range of 700 to 1100°C. The metal/S ratio in the sulfide starting mix was kept at 0.99 to keep the S fugacity constant at around log *f*S2 = -7 in all experiments (e.g., Helmy et al., 2010). We observe that the Pt and Pd show different behavior in the two systems. Immiscible Pt-Sb melt and Pt-Sb minerals are stable at higher temperatures relative to Pd-Sb melt and minerals. The first Pt-Sb and Pd-Sb phases are stable at 980°C and 750°C, respectively. No Pt-Bi or Pd-Bi phases are stable above 780°C. The monosulfide solid solution host very low Sb and Bi contents while sulfide melt dissolves weight % levels of Sb and Bi confirming very low $D_{Sb}^{(mss\text{-}sulfide\ melt)}$ and $D_{Bi}^{(mss\text{-}sulfide\ melt)}$ previously proved by Helmy et al. (2010).

This is a preprint, the final version is subject to change, of the American Mineralogist (MSA)
Cite as Authors (Year) Title. American Mineralogist, in press.
DOI: https://doi.org/10.2138/am-2020-7154

2. Experimental and analytical procedures

Pure metal powders, elemental S, Sb and Bi were used to synthesize the starting mixes. The antimonide and bismuthinide phases were mixed with an $(Fe,Ni,Cu)_{1-x}S$ monosulfide matrix (Table 1) and equilibrated at temperatures between 1,100 and 700°C. The sulfide matrix has a molar metal/S ratio close to unity.

For each experiment, ca. 150 mg of synthesized Fe–Ni– Cu sulfide component and 15 mg of either $PtSb_2$, $PtBi_2$, $PdSb_2$, or $PdBi_2$ were charged into SiO_2 glass tube. The tube was evacuated and welded shut. The capsules were then placed in a vertical furnace at the desired temperatures. Run durations were dependent on the run temperature and ranged from 12 h at 1,100°C to 6 days at 700°C. After the run all capsules were quenched within seconds by dropping them into cold water. Neither oxygen nor sulfur fugacities were adjusted or controlled during the experiment. The presence of sulfide phases within each evacuated quartz ampoule should impose relatively reducing conditions (controlled by the stability of sulfide). The S fugacity was estimated from the mole fraction of FeS in the stable $(Fe, Ni)_{1-x}S$ solid solutions representing the solid sulfide phase during the experiments (cf. Toulmin and Barton 1964; Barin 1995; Bockrath et al. 2004; Helmy et al., 2013a,b). Table 2 summarizes the experimental conditions and phase relations.

Major element compositions were determined using a JEOL JXA 8200 electron microanalyzer at 15 kV and 20 nA, using native Ni, Sb and Bi and natural pyrrhotite,

chalcopyrite, arsenopyrite, and PGE metals as standards. The noble metal phases wre analyzed on the L_a lines at 20 kV. The electron beam was defocused to 30 microns to integrate small-scale chemical heterogeneities caused by exsolution on quench.

3. Phase relations and compositions

3.1 The Pt- and Pd-Sb-sulfide systems

At 1,100°C, our highest temperature experiment, all run products are completely molten. In the Pt-bearing experiments, rounded grains of quenched immiscible PtSb melt of about 50 µm in diameter exist in the sulfide melt. Metastable quench products are dendritic mss, Ni-Cu iss with large grains of antimonides (Fig. 1a). In the Pd-bearing experiments, the PdSb component is fully miscible with the sulfide melt. The Pd-antimonide quench patches are evenly distributed in the sulfide matrix (Fig. 1b).

At 980°C, geversite ($PtSb_2$) is a stable phase in the Pt-bearing experiments (Fig. 1c). It forms euhedral crystals less than 50 µm in diameter set in a matrix of mss. The Fe-Ni-Cu-sulfide melt was quenched to dendritic mss and sulfide-arsenide melt (Fig. 1c). Geversite crystals are commonly hosted in the quenched sulfide melt and have typically an euhedral morphology suggesting that they existed in equilibrium with mss (Fig. 1c). On quench the mss decomposed to smaller mss grains, intermediate solid solution (iss) and bright Ni-Sb grains evenly distributed in the iss. The mss forms large rounded grains rarely hosting geversite crystals.

In the Pd-bearing experiments, immiscible PdSb melt is stable forming rounded grains in the quenched sulfide melt or included in mss (Fig. 1d). The rounded immiscible PdSb melt inside mss suggests that this immiscibility takes place at temperatures above the liquidus of mss, i.e., 1020°C. The sulfide melt quenches to mss, iss and Ni-Sb irregular grains (Fig. 1d).

At 900°C, geversite, mss and sulfide melt are stable phases in the Pt-bearing experiments. Geversite forms small euhderal crystals included in mss or in the quenched sulfide melt (Fig. 1e). Geversite, enveloped in mss, is fine-grained relative to that crystallized in the sulfide melt. The sulfide melt quenches to dendritic mss, iss and small NiSb grains. In the Pd experiments, the immiscible PdSb melt forms rounded grains hosted in the sulfide melt or rarely in mss (Fig. 1f). Mss forms large rounded grains while the sulfide melt quenches to dendritic mss, iss and NiSb grains.

At 830°C, mss, geversite and iss are the stable phases in the Pt-bearing experiments. The mss is relatively large while geversite crystals are smaller than in the 900°C run. In the Pd-bearing experiments, mss, sulfide melt and Pt-Ni-antimonide are stable phases. The Pd antimonide phase forms rounded grains commonly included in the sulfide melt. The rounded shape suggests that this antimonide was a liquid phase during the run.

At 750°C, nickeliferous sudburyite (PdNi)Sb is a stable phase in the Pd-bearing experiments, it forms subhedral grains in iss (Fig. 1g). Sudburyite grains hosted in mss are rounded in shape, they likely crystallized from trapped antimonide melt globules in mss. Mss coexists in equilibrium with iss.

147 Tables 3 and 4 list the compositions of run products in the Pt- and Pd-bearing
148 experiments, respectively. In the Pt-Sb sulfide system at 1100°C, the sulfide melt
149 dissolves 3.8 and 2.9 wt.% Sb and Pt, respectively. The coexisting antimonide melt
150 contains 37 and 60.1 wt%, Sb and Pt respectively (Table 3). The amount of Sb soluble in
151 sulfide melt decreases with decreasing temperature to be 3.1 and 1.8 wt.% Sb at 980
152 and 900°C, respectively. Similarly, the Pt content of the sulfide melt decreases from 1.5
153 wt. % (at 980°C) to 0.5 wt.% (at 900°C). Mss dissolves 0.13 and 0.30 wt.% Pt at 980 and
154 900°C, respectively, while the Sb content is below the EMPA detection limit.
155 The partition coefficients of Cu and Ni between sulfide and antimonide melts at 1100°C
156 are around 2, while Fe strongly partitions to the sulfide melt ($D_{Fe}^{\text{sulfide melt/antimonide melt}}$ =
157 129). Figures 2 and 3 illustrate the distribution of Ni and Cu between mss and the Sb-
158 bearing sulfide melt in the two sets of experiments. While Cu is incompatible over the
159 whole temperature range in the Pt and Pd experiments, Ni behaves as an incompatible
160 element only at high temperatures; above 900°C and 830°C in the Pt-and Pd-
161 experiments, respectively. Pt partitions to the antimonide melt (Figs. 4) with the
162 ($D_{Pt}^{\text{antimonide melt/sulfide melt}}$) at 1100°C of about 21. The $D_{Pt}^{\text{mss/sulfide melt}}$ is around 0.08 at
163 980°C.
164 In the Pd-Sb-bearing sulfide system, the sulfide melt in equilibrium with Sb-melt contains
165 1.2 and 6 wt.% Pd and Sb, respectively at 980°C. The Sb content of the sulfide melt
166 increases to 12 wt.% (at 900°C) and sharply drops to 0.2 wt.% when the solidus of the
167 Pd-Sb rich melt is reached (i.e. between 830°C and 750°C). The Ni content sharply drops

in the iss (Fig. 2). The Pd and Sb contents of mss are equal or below the EMPA detection limits over the whole temperature range explored (Table 4).

Pd partitions to the antimonide phase (Fig. 5) with $D_{Pd}^{\text{antimonide melt/sulfide melt}}$ of 38 at 980°C and 900°C. Ni has slightly higher partition coefficients between antimonide and sulfide melts (0.11 and 0.18 at 980 and 900°C, respectively) relative to Cu (0.07 and 0.05 at 980 and 900°C, respectively). The very low Sb and Pd contents in mss make any calculations of partition coefficients between mss and sulfide melt irrelevant.

3.2. The Pt- and Pd-Bi-sulfide systems

At 1,100°C, only sulfide melt is a stable phase in the Pt and Pd-experiments. No immiscible bismuthinide melts were observed.

At 1,050°C, in the Pt- and Pd-bearing experiments, mss is a stable phase, it forms large rounded grains commonly surrounded by bright Bi-rich areas (Fig. 6a). The sulfide melt quenches to metastable mss and iss and Bi-rich micron-size grains evenly distributed between metastable mss and iss grains. Bi-rich globules are encountered in cavities in the quenched sulfide melt (Fig. 6b). These globules are only noted in cavities in the quenched sulfide melt and, therefore, are likely condensates of a Bi-rich vapor phase. Helmy and Fonseca (2017) interpreted similar Se-rich globules in cavities in the sulfide melt of the Pt- Se-sulfide system as condensate from a vapor phase.

At 980°C, in the Pt- and Pd-experiments, mss and sulfide melt are stable phases. The sulfide melt quenches to small grains of metastable mss and iss and micron-size bright

irregular Bi-rich (60 wt.% Bi, the rest is either Pt or Pd and minor Ni and Cu) grains commonly concentrated at the mss-melt interface. No stable Pt- or Pd-phases are noted. At 900°C, in both Pt- and Pd-experiments, mss forms larger, rounded grains (Fig. 6c, d) in a matrix of sulfide melt. The latter quenches to metastable mss and iss. The sulfide melt hosts sub-micron size bright Bi-rich (65 wt.% Bi, the rest is either Pt or Pd) grains evenly distributed in the groundmass or concentrated around mss grains.

At 830°C, mss and sulfide melt are the stable phases in both sets of experiments (Figs 6e, f). The mss is relatively large in a matrix of the Bi-rich sulfide melt. No bismuthinide phases are stable in the two systems.

At 780°C, in both experiments, the sulfide melt crystallizes to iss. The Bi-rich (> 67 wt.% Bi, the rest is either Pt or Pd phase is completely separated from the iss (Figs. 6g, h). The mss and the Bi-rich areas are larger in size in the Pt-experiments. Insizwaite ($PtBi_2$) is a stable phase; it forms elongated crystals inside a S-rich Pt-bismuthinide melt (Fig. 6i). In the Pd-bearing experiments, the Bi-rich phase does not show exsolution (Fig. 6j), it is a quenched bismuthinide melt. At 700°C, froodite ($PdBi_2$) crystallizes as elongated crystals from the Bi-rich melt (Fig. 6k). Mss and iss are the other stable phases.

The compositions of run products in the Pt and Pd experiments are listed in Tables 5 and 6, respectively. The Bi and Pt contents of mss in Pt-experiments are constant around 0.2 and 0.3 wt.%, respectively, over the whole temperature range. In the coexisting sulfide melts, the Bi and Pt contents increase with the falling temperature until the solidus of the first bismuthinide phase is reached at 780°C. The Bi content of iss equilibrated with

insizwaite (in the Pt experiments and the Bi-rich melt (in the Pd experiment) drops to 0.15 wt.%. Figures 7 and 8 illustrate the distribution of Ni and Cu between mss and the Bi-bearing sulfide melt. While Ni behave incompatible above the sulfide solidus and incompatible below 830°C, Cu stays incompatible over the whole temperature range, with $D_{Cu}^{mss/sulfide\ melt}$ increase at lower temperatures. The Fe, Ni and Cu contents of the crystalline Pt-bismuthinide phase at 780°C are very low (Table 5), while the Pd-bismuthinide melt at the same temperature accommodates high Fe, Ni and Cu (Table 6). In the presence of Bi, both Pt and Pd behave as highly incompatible between mss and Bi-rich melt (Fig. 9). Both elements partition to the Bi-rich phase when it separates from the iss below 780°C. Similarly, Bi is highly incompatible in mss and iss; it partitions into the sulfide melt at high temperatures until the solidus of the iss is reached, and partitions to a bismuthinide melt phase when iss is stable phase.

4. Discussion

During the evolution of the Pt- and Pd-Sb-bearing sulfide melts, Pt and Pd partition to an immiscible antimonide melt. The D_{Pt} and D_{Pd} (antimonide melt/sulfide melt) are around 20 and 40, respectively. The liquids of the Pt-antimonide is above 980°C, while that of Pd is slightly above 750°C. Nickel and Cu have stronger affinity to sulfide melt, indicated by their low $D_{Ni}^{antimonide\ melt/sulfide\ melt}$ and $D_{Cu}^{antimonide\ melt/sulfide\ melt}$ (0.13 and 0.15, respectively). The affinity of Ni to the antimonide melt increases with cooling in the Pd-experiments, but the $D_{Ni}^{(antimonide\ melt/sulfide\ melt)}$ is always <0.4.

Unlike Sb (and As, Helmy et al., 2013a), Bi partitions to a vapor phase at 1050°C; no immiscible bismuthide melt forms above the solidus of the sulfide melt. Bismuth is fully miscible in the sulfide melt and the high Bi content of the sulfide melt increases the solubility of Pt and Pd but does not influence the behavior of Ni, which partitions to mss. Indeed, the behavior of Pt, Pd and Ni in the Bi-sulfide systemic is very similar to their behavior in the Se-sulfide system (Helmy and Fonseca, 2017).

4.1. Comparison with other semi-metal sulfide systems

A similar feature of the Sb-sulfide system and the As-sulfide system (Helmy et al., 2013a) is that both As and Sb form immiscible melts. In addition, the behavior of Pt and Pd is very similar in both systems (Pt and Pd are highly compatible in the arsenide melt with D_{Pt} and $D_{Pd}^{\text{arsenide melt/sulfide melt}}$ of 40 and 18, respectively; Helmy et al., 2013a). On the other hand, Ni shows stronger affinity to the arsenide melt than to the antimonide melt with $D_{Ni}^{\text{arsenide melt/sulfide melt}} > 1$ compared with $D_{Ni}^{\text{antimonide melt/sulfide melt}} < 0.4$ over the whole temperature range of the Pd experiments. Phase chemistry of the antimonide and arsenide systems suggests that the affinity of Pt and Pd to As and Sb are similar.

The Bi-system is similar to the Se-system in that no immiscible selenide melt forms down to 780°C, in addition Se, like Bi, partitions to a vapor phase (Helmy and Fonseca, 2017). The Bi and Se contents of the sulfide melt increase with decreasing temperature until the sulfide melt crystalizes to iss. While the Bi content of the iss significantly drops due to the formation of Bi-rich melt, the Se content stays high in the iss, because Se is

incorporated in solid solution in the iss. Pt and Pd-bismuthoides and selenides have the lowest thermal stabilities among other platinum group minerals (PGM).

In all systems, Pt and Pd behave incompatibly during the evolution of the semimetal-bearing sulfide melt. The Pt-phases (melts or crystalline) are of higher thermal stabilities than Pd-phases (melts or crystalline), for example, Pt-arsenides, antimonies, tellurides and bismithinides are of higher thermal stability than the corresponding Pd-phases (Helmy et al., 2007, 2013a; Helmy and Fonseca, 2017). The Pt-Te, Pt-As and Pt-Sb immiscible melts appear at temperatures higher than the Pd-Te, Pd-As and Pd-Sb miscible melts. There is distinct difference in Pt-semimetal phase stability among systems; Pt-As phase have the highest thermal stability (sperrylite, 1230°C), followed by Pt-Sb (geversite, 980°C), Pt-Te (moncheite, 920°C), Pt-Bi (insizwaite, 780°C). No Pt-Se phases are stable above 700°C, the lowest run temperature. All Pd-semimetal crystalline phases have thermal stabilities below 750°C.

4.2. Implications on PGM formation from sulfide melts

Platinum and Pd commonly form discrete PGM phases with As, Sb, Te and Bi in magmatic and hydrothermal sulfide deposits (e.g. Cawthorn et al., 2002; Barkov et al., 20002; Helmy, 2004, 2005; McDonald, 2008; Godel et al., 2007; Holwell and McDonal, 2007; Spiridonov et al., 2015 and many others). PGE substitution in sulfide minerals is very limited whenever semimetals are available (Gervilla et al., 1998; Holwell and McDonald, 2007; Hutchinson and McDonald, 2008). The Pt, Pd, Sb and Bi contents of our

experimental runs are much higher than their abundances in natural sulfide-bearing magmas and sulfide liquids. The (Pt + Pd)/ (Te + Sb + Bi) weight ratios of some massive magmatic sulfides are in the range of ~0.2–0.3 (e.g., Piña et al. 2006). These natural ratios are lower than that in our experiments. The recent experimental (Helmy et al., 2013b) and mineralogical (e.g. Maier et al., 2015; Barnes et al., 2016, Kamenetsky et al., 2016) evidence of PGM crystallization from melts and magmas highly undersaturated in PGE and semimetals highlights the strong preference of PGE to semimetals at magmatic conditions as suggested earlier by Tredoux et al (1995). Probably, the low (Pt + Pd)/(Te + Sb + Bi) bulk ratios in nature keep Pt and Pd as long as possible dissolved in the sulfide melt as PGE-semimetal associations (Helmy et al., 2013b) until a discrete immiscible semimetal melt can exsolve (Helmy et al., 2007). These immiscible melt droplets are exsolved from late-stage fractionation of sulfide melt (e.g. Graham et al., 2017) just before the solidus of sulfide melt is reached. Although the experiments are made with wt.% levels of PtSb and PdSb, antimonide and bismuthide liquid immiscibility likely happens also at much lower concentrations by analogy to other systems (e.g. the Pt-As sulfide system, Helmy et al., 2013b). Helmy et al (2013b) observed nanometer-size immiscible Pt-As melt in sulfide melt highly undersaturated with Pt arsenide.

It is commonly suggested that PGM, apart from alloys, form during cooling and recrystallization of primary sulfide minerals within which the PGE were originally dissolved in solid solution (e.g., Ballhaus and Ulmer, 1995, Peregoedova and Ohnenstetter 2002, Peregoedova et al. 2004,). The only supporting evidence of this suggestion is the high

294 PGE content in some common sulfide minerals, although this is always true.
295 Chalcopyrite, for example, hardly ever contains PGE that aren't in the form of discrete
296 PGM. In addition to textural evidence arguing against exsolution mechanism (Godel et
297 al., 2010), there is no guarantee that these high PGE contents are not due to
298 submicroscopic inclusions. In harmony with previous estimates of low solubility of Sb
299 and Bi in mss (Helmy et al., 2010), the EMP analyses of mss from the experiments
300 revealed constantly low Sb and Bi contents (Tables 3-6). The low concentrations of Sb
301 and Bi in mss over the whole explored temperature range suggests that Pt and Pd
302 antimonides and bithmusthinides are not likely to form by exsolution from mss during
303 cooling as previously suggested (e.g. Ballhaus and Ulmer, 1995). The highly incompatible
304 behavior of Pd, Sb and Bi (and Te) during evolution of sulfide liquids and the low thermal
305 stabilities of Pd-semimetal phases will lead to their enrichment in the late fractionated
306 sulfide melt. The results of the present study imply that Sb and Bi form tiny immiscible
307 globules that scavenge Pd and are expelled out of sulfide melt during cooling (e.g.
308 Holwell and McDonald, 2007, Helmy et al., 2007). This explain the many Pd-Sb and Pd-Bi
309 (and Pd-Te) minerals known in deposits of extensive late-magmatic, metasomatic or
310 hydrothermal history (e.g. Noril'sk sulfide ores, Spiridonov et al., 2015, and the Sudbury
311 footwall ores, Pentek et al., 2008) and supports the assumption (Ebel and Naldrett,
312 1996; Prichard et al., 2004) that PGE antimonides and bismuthinides could form directly
313 from the fractionating immiscible sulfide liquids over quite a large temperature range
314 (McDonald, 2008). In addition, the compatible behavior of IPGE (Ir, Os, Ru) during the

315 evolution of sulfide liquid (they strongly partition to mss) explains the scarcity of IPGE-Sb
316 and IPGE-Bi phases in magmatic sulfide deposits.
317
318 Although Ni-antimonides (e.g. nisbite, $NiSb_2$, breithauptite NiSb) and sulfantimonides
319 (ullmanite NiSbS, tucekite, $Ni_9Sb_2S_8$) are known in nature (e.g. the Platreef at Turfspruit,
320 Hutchinson and Kinnarid, 2005), they did not form in our experiments although Ni and
321 Sb are major components of the systems. It is clear that the affinity of Sb to combine
322 with Pt and Pd is higher than its affinity to combine with Ni. In addition, the low Ni
323 content of the Pt-Sb phase and the high Ni content of the Pd-Sb phase (Tables 2,3) points
324 to a temperature factor, the Ni-Sb phases are only stable at relatively lower
325 temperatures than the Pt-Sb and Pt-Pd phases. Probably Ni-antimonides form only at
326 low temperatures and high Sb/(Pt + Pd) ratio in the ore forming fluids. Hutchinson and
327 Kinnarid (2005) suggest that the several Ni antimonide phases in the Platreef at Turfspuit
328 were formed by an increase in the Sb/(Pt+Pd) ratio caused by low-temperature
329 hydrothermal fluids.
330
331 **4.3. The role of Bi melt in hydrothermal, porphyry and skarn systems**
332 The role of low temperature Bi (and Te) melts in scavenging Au, Ag and Pd at relatively
333 low temperatures has been proposed for some hydrothermal gold deposits (Hein et al.
334 2006), skarn deposits (Cockerton and Tompkins 2012) and porphyry systems (McFall et
335 al 2018). For example, in the Skouries Cu-Au (Pd, Pt, Te) porphyry deposit, an immiscible

Bi-Te melt scavenged precious metals leading to the formation of several Pt and Pd-antimonide and bismuthotellurides (McFall et al., 2018). Hein et al (2006) noted the intimate association of gold with Bi in vapor-liquid phase in fluid inclusions in quartz veins from the Batman deposit, Mt. Todd (Yimuyn Manjerr) goldfield, Australia. In the Bi-Au Stormont skarn prospect, Northwest Tasmania, Au is associated with various Bi-phases formed during metasomatism (Cockerton and Tompkins 2012). The common association of Au with Bi led Douglas et al (2000) to propose the Liquid Bismuth Collector Model, which involves the scavenging of Au from hydrothermal fluid by the liquid bismuth. Our experiments are made in closed Cu-Ni-Pt-Pd sulfide system and do not contain Te but the proved volatility of Bi and the low-temperature stability of Bi-melt have bearing in the hydrothermal-porphyry systems. In addition to the proved Bi volatility and Bi-melt stability at low temperatures, the proved strong affinity of precious metals to the melt, may explain the role played by Bi melts in scavenging precious metals in hydrothermal gold deposits, porphyry and skarn systems.

4.4. Petrologic implications

The extremely low contents of Bi and Sb in mss in the experimental run products and the incompatible behavior of both elements during the solidification of the sulfide melt, suggest that Bi and Sb host phases, apart from geversite, are low-temperature phases. As suggested by Jenner (2017), these low-temperature phases will be unstable during subduction processes. The low Sb and Bi contents in sulfide inclusions in eclogitic

357 diamonds that are believed to have formed in the cratonic keel following some kind of
358 subduction process suggests that these elements may have been lost during subduction
359 (see Aulbach et al 2012; McDonald et al 2017). The strong incompatible behavior of Sb
360 and Bi during sulfide liquid evolution means that low-degrees of partial melting of
361 sulfide-bearing mantle will lead to the mobilization of both elements. Low-degrees of
362 mantle partial melting and mantle metasomatism involving sulfide component will
363 produce and segregate a Cu-rich sulfide melt enriched in Bi, Sb, (and Te, Helmy et al.,
364 2007) (e.g. Luguet et al., 2003). Luguet et al (2003) documented high semimetals and Te
365 in mantle derivatives produced by low (2-4%) degrees partial melting. Physical extraction
366 of the Cu-rich sulfide melt along with the silicate melt (Ballhaus et al., 2006) will produce
367 a basalt enriched in these elements and with low As/Sb ratios relative to the primitive
368 mantle.
369 Helmy et al (2013b) presented strong experimental evidence that PGM are preceded by
370 nano-associations (complexes, clusters or nano-crystals) in the sulfide melt and that
371 these nano associations act as fundamental building blocks for the growth of the liquidus
372 PGM. The nano associations mimic the composition of the crystalline phase and their
373 stability in the melt depend on the thermal stability of the macroscopic phase. Helmy
374 and Bragagni (2017) introduced the term selective complexing as a possible cause of PGE
375 fractionation in nature. For example, while As can fractionate PGE (Helmy et al., 2013b;
376 Helmy and Bragagni, 2017), Se has no role in the fractionation of PGE in nature, because
377 it does not form stable complexes with any of the PGE at magmatic conditions (Helmy

and Fonseca, 2017). The results presented here suggest that Bi, like Se, will have no role in Pt and Pd fractionation in nature, simply because Bi-Pt and Bi-Pd phases are only stable below the solidus of the iss. On the other hand, Sb, like Te and As can fractionate Pt from Pd in magmatic sulfide ores (because these elements form stable phases with Pd, only at lower temperatures; i.e., below the solidus of the iss).

Conclusions

Antimony, like As, will capture Pt and Pd from sulfide melt and form immiscible antimonide melt. Both Pt and Pd-antimonides crystallize directly from the immiscible antimonide melt. Bismuth, like Se, partitions to a vapor phase at temperatures above 1050°C and is highly soluble in sulfide melt, until the later crystallizes into iss. Pt- and Pd-bismuthinides crystallize directly from Bi-rich melt at 780 and 700C°C, respectively. The present study adds experimental evidence for the notion that Pt and Pd antimonides form by direct crystallization from droplets of immiscible Sb-enriched melt and not by exsolution from sulfide phase. Pt- and Pd-bismuthinides crystallize from Bi-rich melt below the solidus of the sulfide melt. Antimony and Bi are likely to be highly mobile in the mantle during partial melting, especially if melting involves a sulfide melt; the concentration of Bi in the vapor phase and the late-magmatic and hydrothermal fluids is likely to be high. Antimony can fractionate Pt from Pd during the evolution of sulfide liquids while Bi cannot.

Acknowledgments

H.M. Helmy's research was funded by the Alexander von Humboldt Society through a Georg Forster Research Award. We thank Iain McDonald and another anonymous reviewer for critical comments on the manuscript and Kate Kiseeva for editorial handling.

References

Aulbach S, Stachel T, Seitz H.-H, Brey G (2012) Chalcophile and siderophile elements in sulphide inclusions in eclogitic diamonds and metal cycling in a Paleoproterozoic subduction zone**.** Geochim Cosmochim Acta 93:278-299.

Ballhaus C, Bockrath C, Wohlgemuth-Ueberwasser C, Laurenz V, Berndt J (2006) Fractionation of the noble metals by physical processes. Contrib Mineral Petr 152:667–684.

Ballhaus C, Ulmer P (1995) Platinum-group elements in the Merensky reef. II. Experimental solubility of Pt and Pd in synthetic $Fe_{1-x}S$ between 950 and 450° under controlled f_{S2} and f_{H2}. Geochim Cosmochim Acta 59:4881–4888

Barin I (1995) Thermochemical data of pure substances. Weinheim, New York.

Barkov AY, Laflamme JHG, Cabri LJ, Martin RF (2002) Platinum-group minerals from the Welgreen Ni–Cu–PGE deposit, Yukon, Canada. Can Mineral 40:651–669

Barnes S J, Fisher L A, Godel B, Pearce M A, Maier W D, Paterson D, Howard D L, Ryan C, Laird J S (2016) Primary cumulus platinum minerals in the Monts de Cristal complex,

Gabon, magmatic microenvironments inferred from high-definition X-ray fluorescence microscopy. Contrib. Mineral. Petrol. 171(3), 1–18.

Bockrath C, Ballhaus C, Holzheid A (2004) Fractionation of the platinum-group elements during mantle melting. Science 305, 1951–1953.

Cawthorn RG, Lee CA, Schouwstra RP, Mellowship P (2002) Relationship between PGE and PGM in the Bushveld Complex. Canadian Mineralogist, 40, 311–328.

Cockerton A, Tompkins A (2012). Insights into the liquid bismuth collector model through analysis of the Bi-Au Stormont Skarn Prospect, Northwest Tasmania. Economic Geology 107, 667-682.

Douglas N, Mavrogenes J, Hack A, England R. (2000) The liquid bismuth collector model: an alternative gold deposition mechanism. Geological Society of Australia Abstracts No. 59, 15th Australian Geological Convention, Sydney, July 2000.

Ebel DS, Naldrett AJ (1996) Fractional crystallization of sulfide ore liquids at high temperature: Economic Geology 91, 607–621.

Gervilla F, Papunen H, Kojonen K, Johanson B (1998) Platinum, palladium, and gold-rich arsenide ores from the Kylmakoski Ni–Cu deposit (Vammala Nickel Belt, SW Finland). Mineralogy and Petrology 64:163–185

Godel B, Barnes SJ, Barnes S-J, Maier D (2007) Platinum-Group Elements in Sulfide Minerals, Platinum-Group Minerals, and Whole-Rocks of the Merensky Reef (Bushveld Complex, South Africa): Implications for the Formation of the Reef. Journal Petrology 48, 1569-1604.

441 Godel B, Barnes SJ, Barnes S-J, Maier D (2010) Platinum ore in three dimensions: insights
442 from high-resolution X-ray computed tomography. Geology 38:1127–1130
443 Graham SD, Holwell DA, McDonald I, Jenkin GRT, Hill NJ, Boyce AJ, Smith J, Sangster C
444 (2017) Magmatic Cu-Ni-PGE-Au sulfide mineralisation in alkaline igneous systems: An
445 example from the Sron Garbh intrusion, Tyndrum, Scotland. Ore Geology Reviews 80,
446 961–984
447 Hattori KH, Arai S, Clarke DB (2002) Selenium, tellurium, arsenic and antimony contents
448 of primary mantle sulfides. Canadian Mineralogist, 40, 637–650
449 Hein K, Zaw K, Mernagh T (2006) Linking mineral and fluid inclusion paragenetic studies:
450 The Batman deposit, Mt. Todd (Yimuyn Manjerr) goldfield, Australia. Ore Geology
451 reviews 28, 180-200.
452 Helmy HM (2004) Cu-Ni-PGE mineralization in the Genina Gharbia mafic-ultramafic
453 intrusion, Eastern Desert, Egypt. Canadian Mineralogist, 42 (2), 351-370.
454 Helmy HM (2005) Melonite group minerals from three Cu-Ni-PGE prospects, Eastern
455 Desert, Egypt. Ore Geology Reviews, 26, 305-324.
456 Helmy HM, Bragagni A (2017) Platinum-group elements fractionation by selective
457 complexing: the Os, Ir, Ru, Rh-arsenide-sulfide systems above 1020°C. Geochimica
458 et Cosmochimica Acta 216, 169-183.

Helmy HM, Fonseca R (2017) The behavior of Pt, Pd, Cu and Ni in the Se-sulfide system between 1050 and 700°C and the role of Se in platinum-group elements fractionation in sulfide melts. Geochimica et Cosmochimica Acta 216, 141-152.

Helmy HM, Stumpfl EF, Kamel OA (1995) Platinum group minerals from the metamorphosed Abu Swayel Cu-Ni-PGE mineralization, South Eastern Desert, Egypt. Economic Geology, 90: 2350-2360.

Helmy HM, Ballhaus C, Berndt J, Bockrath C, Wohlgemuth-Ueberwasser C (2007) Formation of Pt, Pd and Ni tellurides: experiments in sulfide–telluride systems. Contributions Mineralogy and Petrology, 153, 577–591.

Helmy HM, Ballhaus C, Wohlgemuth-Ueberwasser, C, Fonseca ROC, Laurenz V (2010) Partitioning of Se, As, Sb, Te and Bi between monosulfide solid solution and sulfide melt – application to magmatic sulfide deposits. *Geochimica et Cosmochimica Acta* 74, 6174-6179.

Helmy HM, Ballhaus,C, Fonseca R, Wirth R, Nagel T, Tredoux M (2013) Noble metal nanoclusters and nanoparticles precede mineral formation in magmatic sulfide melts. Nature Communications 4:2405. DOI:10.1038/ncomms3405

Helmy HM, Ballhaus C, Fonseca R, Nagel T (2013) Fractionation of platinum, palladium, nickel, and copper in sulfide–arsenide systems at magmatic temperature. Contributions to Mineralogy and Petrology, 166, 1725-1737.

478 Holwell D, McDonald I (2007) Partitioning of platinum group elements in the Platreef at
479 Overysel, northern Bushveld Complex: a combined PGM and LA ICP–MS study.
480 Contrib. Mineralogy and Petrology154, 171–190.
481 Hutchinson D, Kinnaird J (2005) Complex multistage genesis for the Ni–Cu–PGE
482 mineralisation in the southern region of the Platreef, Bushveld Complex, South
483 Africa. Applied Earth Science, 114, B208-B224.
484 Hutchinson D, McDonald I (2008) Laser ablation ICP-MS study of platinum-group
485 elements in sulfides from the Platreef at Turfspruit, northern limb of the Bushveld
486 Complex, South Africa. Mineral Deposita 43:695–711
487 Jenner FE (2017) Cumulate causes for the low contents of sulfide-loving elements in the
488 continental crust. Nature Geoscience 10, 524-529.
489 Kamenetsky VS, Park J.-W, Mungall JE, Pushkarev E V, Ivanov AV, Kamenetsky MB, Yaxley
490 GM (2015) Crystallization of platinum-group minerals from silicate melts, Evidence
491 from Cr-spinel–hosted inclusions in volcanic rocks. Geology 43, 903–906.
492 Luguet A, Lorand J-P, Seyler M (2003) A coupled study of sulfide petrology and highly
493 siderophile element geochemistry in abyssal peridotites from the Kane Fracture Zone
494 (MARK area, Mid-Atlantic ridge). Geochim Cosmochim Acta 67:1553−1570
495 Maier WD, Rasmussen B, Fletcher I, Godel B, Barnes SJ, Fisher L, Yang S H, Huhma H,
496 Lahaye Y (2015) Petrogenesis of the 277Ga Monts de Cristal Complex, Gabon,
497 evidence for direct precipitation of Pt-arsenides from basaltic magma. J. Petrol. 56,
498 1285-1308.

McDonald I (2008) Platinum-group element and sulfide mineralogy in ultramafic complexes at western Andriamena, Madagascar. Applied Earth Science (Trans. Inst. Min. Metall. Sect. B) 117, B1–B10.

McDonald I, Hughes H, Butler I, Harris B, Muir D (2017) Homogenisation of sulphide inclusions within diamonds: A new approach to diamond inclusion geochemistry. Geochim. Cosmochim. Acta 216, 335-357.

McFall NJ, Roberts S, Baker T, Spratt J, McDonald I (2018) Platinum-group minerals in the Skouries Cu-Au (Pd, Pt, Te) porphyry deposit. Ore Geology Reviews 99, 364-384.

Noll PD, Newsom HE, Leeman WP, Ryan JG (1996) The role of hydrothermal fluids in the production of subduction zone magmas: evidence from siderophile and chalcophile trace elements and boron. *Geochim. Cosmochim. Acta* **60**, 587-611.

O'Driscoll B, González-Jiménez JM (2016) Petrogenesis of the Platinum-Group Minerals. Rev. Mineral. Geochem., 81, 489-578.

Peregoedova A, Ohnenstetter M (2002) Collectors of Pt, Pd and Rh in an S-poor Fe-Ni-Cu-sulfide system at 760°C: experimental data and application to ore deposits. Canad. Mineral 40, 527-561.

Peregoedova A, Barnes SJ, Baker DR (2004) The formation of Pt-Ir alloys and Cu-Pd-rich sulfide melts by partial desulfurization of Fe-Ni-Cu sulfides: Results of experiments and implications for natural systems. Chem. Geol. 208, 247-264.

Petnek A, Molanr F, Watkinson D, Jones P (2008) Footwall-type Cu-Ni-PGE Mineralization in the Broken Hammer Area, Wisner Township, North Range, Sudbury Structure. Econ. Geol, 103, 1005–1028

Piñ̃a R, Gervilla F, Ortega L, Lunar R (2008) Mineralogy and geochemistry of platinum-group elements in the Aguablanca Ni–Cu Deposit (SW Spain). Mineral Petrol 92, 259-282.

Prichard HM, Barnes SJ, Maier WD, Fisher PC (2004) Variations in the nature of the platinum-group minerals in a cross- section through the Merensky reef at Impala Platinum: Implications for the mode of formation of the reef. Can Mineral 42:423–437

Scambelluri M, Pettke T, Rampone E, Godard M, Reusser E (2014) Petrology and trace element budgets of high-pressure peridotites indicate subduction dehydration of serpentinized mantle (Cima di Gagnone, Central Alps, Switzerland). J. Petrol. 55, 459-498.

Spiridonov EM, Kulagov EA, Serova AA, Kulikova IM, Korotaeva NN, Sereda E, Tushentsova I, Belyakov S, and Zhukov N (2015) Genetic Pd, Pt, Au, Ag, and Rh Mineralogy in Noril'sk Sulfide Ores. Geology of Ore Deposits, 57 (5), 402–432

Toulmin Jr, Barton PN (1964) A thermodynamic study of pyrite and pyrrhotite. Geochim. Cosmochim. Acta 28, 641– 671.

Tredoux M, Lindsay MN, Davies G, McDonald I (1995) The fractionation of platinum-group elements in magmatic systems, with the suggestion of a novel causal mechanism. South African Journal of Geology 98, 157–167.

Figure Captions

Fig. 1. Phase relations of the experiments in back-scattered electron (BSE) mode of the Pt-Sb (left) and Pd-Sb (right) sulfide systems, numbers on the top right of images correspond to run temperatures. (**A**) immiscible antimonide and sulfide melts, note the tiny bright Pt-Sb-rich grains exsolved during quenching of the sulfide melt (PtSb-1100°C). (**B**) Quenched Pd-Sb-bearing sulfide melt, note the regular distribution of the tiny bright Pd-Sb specs (PdSb-1100°C). (**C**) Rounded mss and euhedral geversite in quenched Sb-bearing sulfide melt (PtSb-980°C). (**D**) Rounded mss grains and immiscible antimonide and sulfide melts, the latter quenches to metastable mss and Pd-Sb specs (PdSb-980°C). (**E**) Large rounded mss, fine-grained geversite and quenched sulfide melt; note the larger size of geversite hosted in the quenched sulfide melt relative to that enveloped in mss (Pt-900°C). (**F**) Large mss in a matrix of immiscible Pd-Sb and sulfide melts; the latter quenches to metastable mss (dark-grey) and Pd-Sb-rich sees (PdSb-900°C). (**G**) Subhedral nickeliferous sudburyite (PdNi)Sb, rounded mss and iss (PdSb-750°C).

Figure 2. Distribution of Ni between coexisting mss crystals (*filled squares*) and sulfide melt (*open squares*) in sulfide saturated with PtSb (**A**) and with PdSb melt (**B**). Error bars are 2σ of the mean.

Figure 3. Distribution of Cu between coexisting mss crystals (*filled squares*) and sulfide melt (*open squares*) in sulfide saturated with PtSb (**A**) and with PdSb melt (**B**). Error bars are 2σ of the mean.

Figure 4. Fractionation of Pt between sulfide melt (**A**) and geversite (**B**); at 1100°C the stable Pt antimonide is an immiscible melt. The large *error bars* (2 sigma of the mean) of Pt in sulfide reflect the heterogeneous distribution after quenching of Pt antimonide components dissolved in sulfide melt.

Figure 5. Fractionation of Pd between sulfide melt (**A**) and antimonide melt (**B**); at 1100°C the the Pd antimonide is completely miscible in sulfide melt. The large *error bars* (2 sigma of the mean) of Pd in sulfide reflect the heterogeneous distribution after quenching of Pd antimonide components dissolved in sulfide melt

Fig. 6. Phase relations of the experiments in back-scattered electron (BSE) mode of the Pt-Bi (left) and Pd-Bi (right) sulfide systems, numbers on the top right of images

correspond to run temperatures. (**A**) rounded mss in a matrix of Bi-Pt-bearing sulfide melt (PtBi-1050°C). (**B**) Bi-Pd-rich globules in voids in the quenched sulfide melt (PdBi-1050°C). (**C**) Rounded mss in quenched Bi-Pt—bearing sulfide melt, the sulfide melt quenches to metastable mss (dark-grey) and Bi-rich iss (PtBi-900°C). (**D**) Subrounded mss grains and Bi-Pd-bearing sulfide melt, the latter quenches to metastable mss and Pd-Bi iss (PdBi-900°C). (**E, F**) Large rounded mss in a matrix of quenched Bi-rich sulfide melt, (PtBi-830°C and PdBi-830°C, respectively). (**G, H**) complete separation of the Bi-rich melt and iss with large mss grains (PtBi-780°C and PdBi-780°C, respectively. (**I**) details of a large Bi-rich melt at 830°C, note the euhedral crystals of insizwaite (PtBi2) crystallizing from the Bi-rich melt. (**J**) details of the P-Bi melt of the 780°C run of the PdBi-780°C experiment. (**K**) The Pd-Bi melt crystallizes to froodite (PdBi2), the black dots are Cu-Fe sulfide (PdBi-700°C).

Figure 7. Distribution of Ni between coexisting mss crystals (*filled squares*) and sulfide melt (*open squares*) in sulfide saturated with PtBi (**A**) and with PdBi melt (**B**). Error bars are 2σ of the mean.

Figure 8. Distribution of Cu between coexisting mss crystals (*filled squares*) and sulfide melt (*open squares*) in sulfide saturated with PtBi (**A**) and with PdBi melt (**B**). Error bars are 2σ of the mean.

598

599 Figure 9. Distribution of Pt and Pd between coexisting mss crystals (*filled squares*) and
600 sulfide melt (*open squares*) in sulfide saturated with PtBi (A) and with PdBi melt (**B**).
601 Error bars are 2σ of the mean.

602

603

604

This is a preprint, the final version is subject to change, of the American Mineralogist (MSA)
Cite as Authors (Year) Title. American Mineralogist, in press.
DOI: https://doi.org/10.2138/am-2020-7154

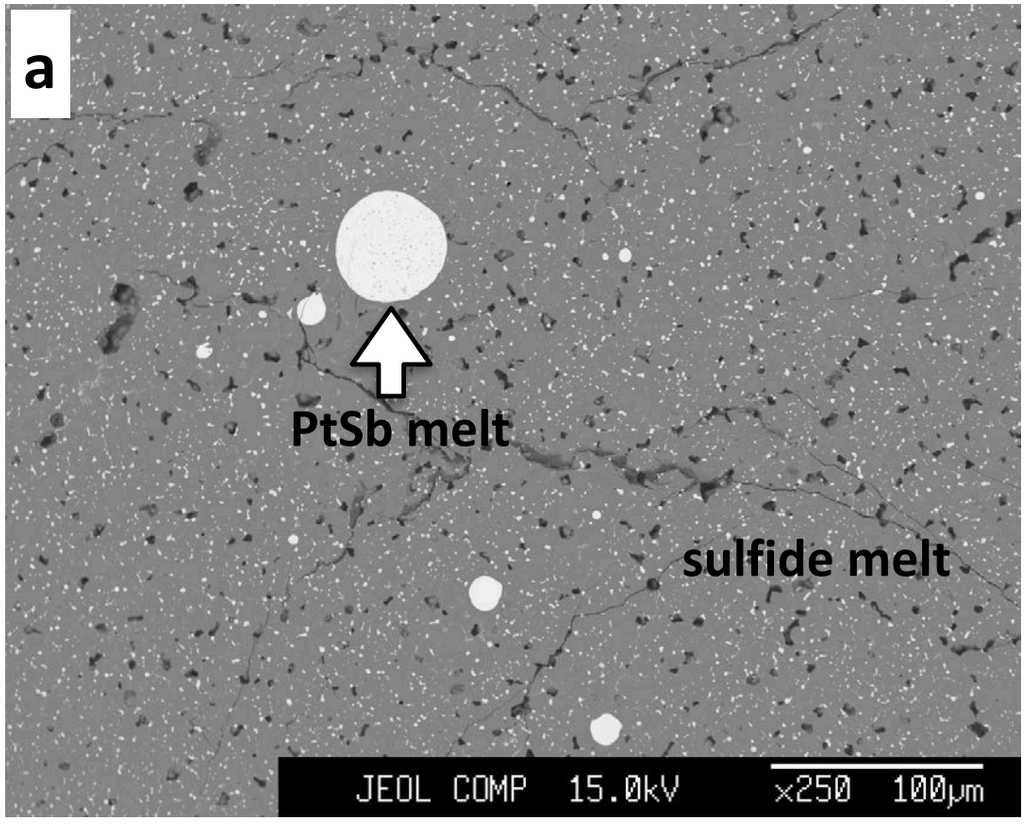

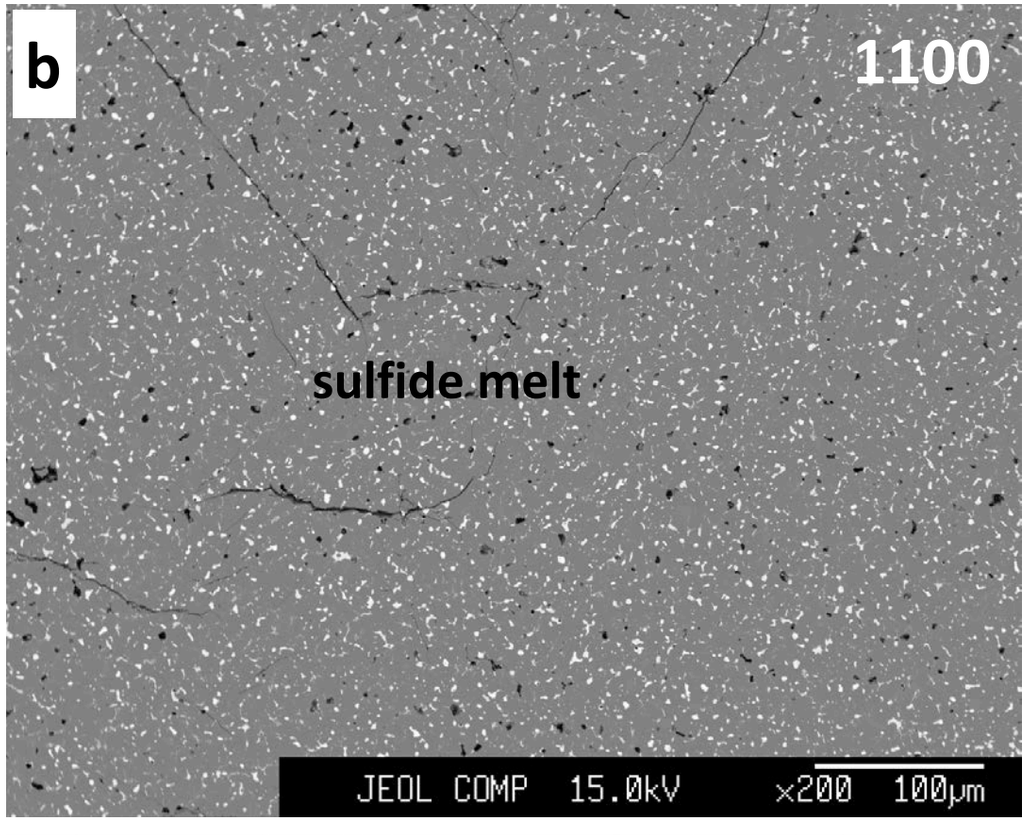

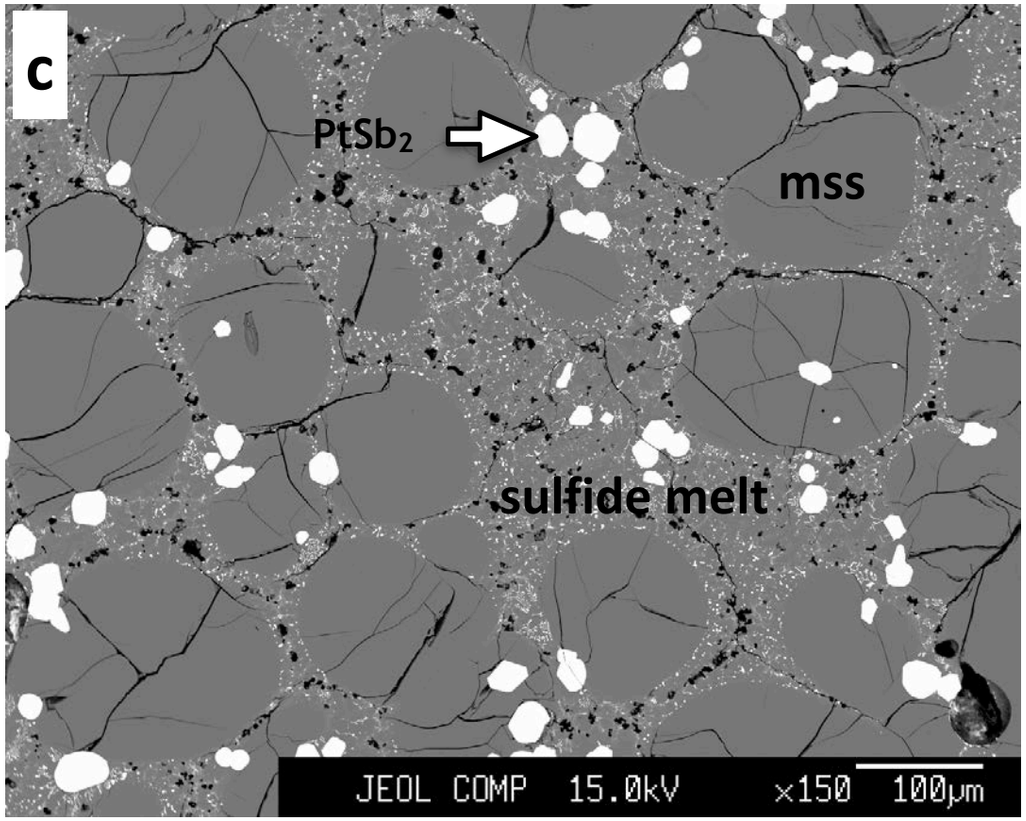

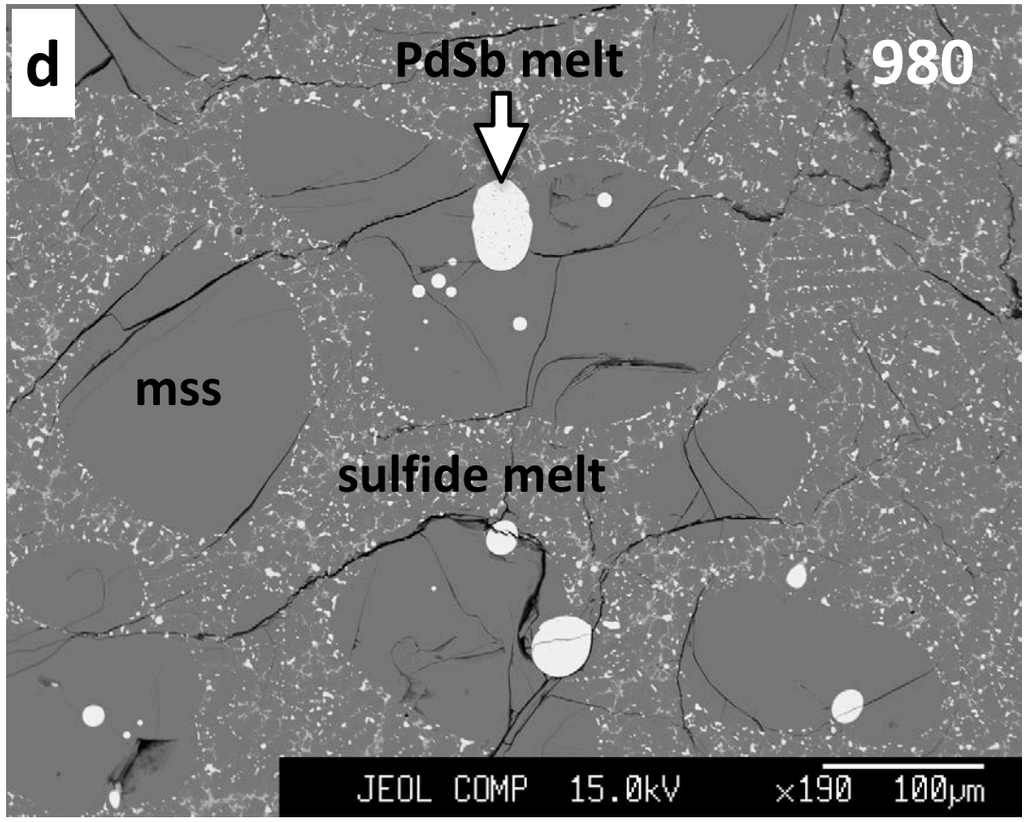

This is a preprint, the final version is subject to change, of the American Mineralogist (MSA)
Cite as Authors (Year) Title. American Mineralogist, in press.
DOI: https://doi.org/10.2138/am-2020-7154

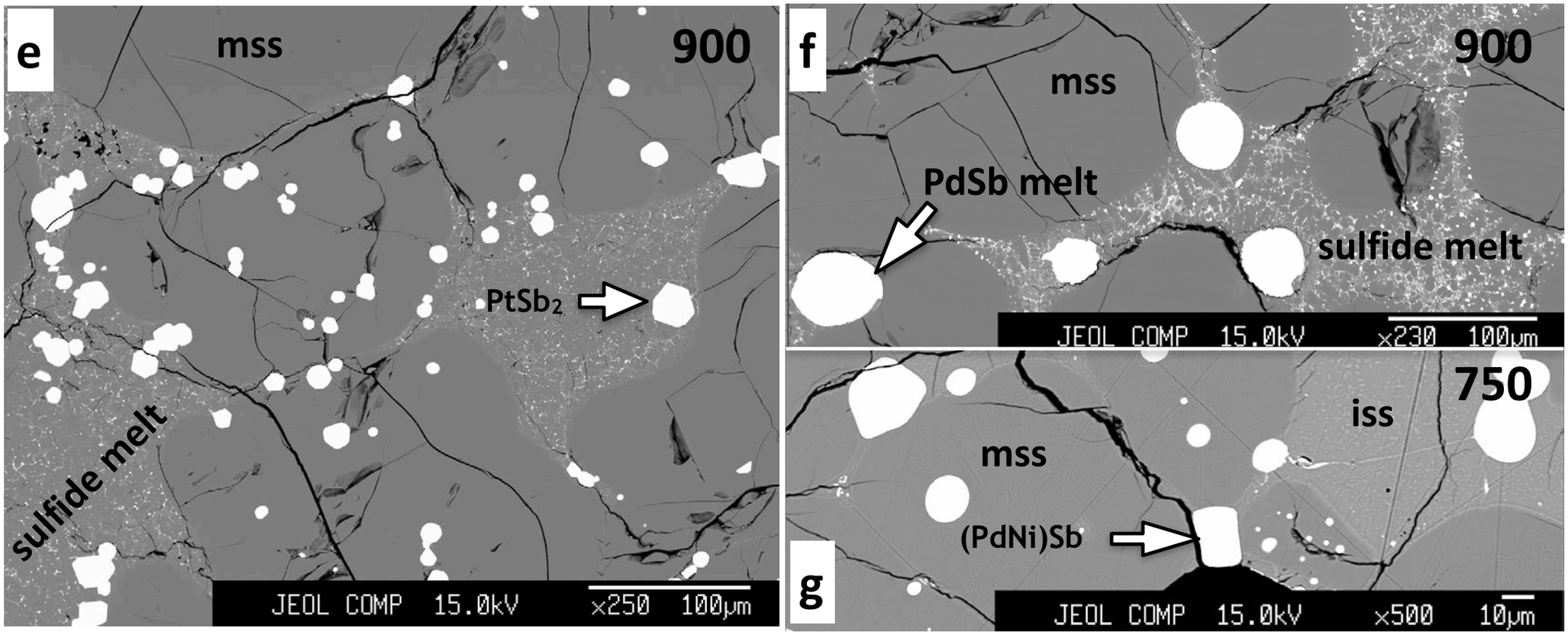

Figure 1

This is a preprint, the final version is subject to change, of the American Mineralogist (MSA)
Cite as Authors (Year) Title. American Mineralogist, in press.
DOI: https://doi.org/10.2138/am-2020-7154

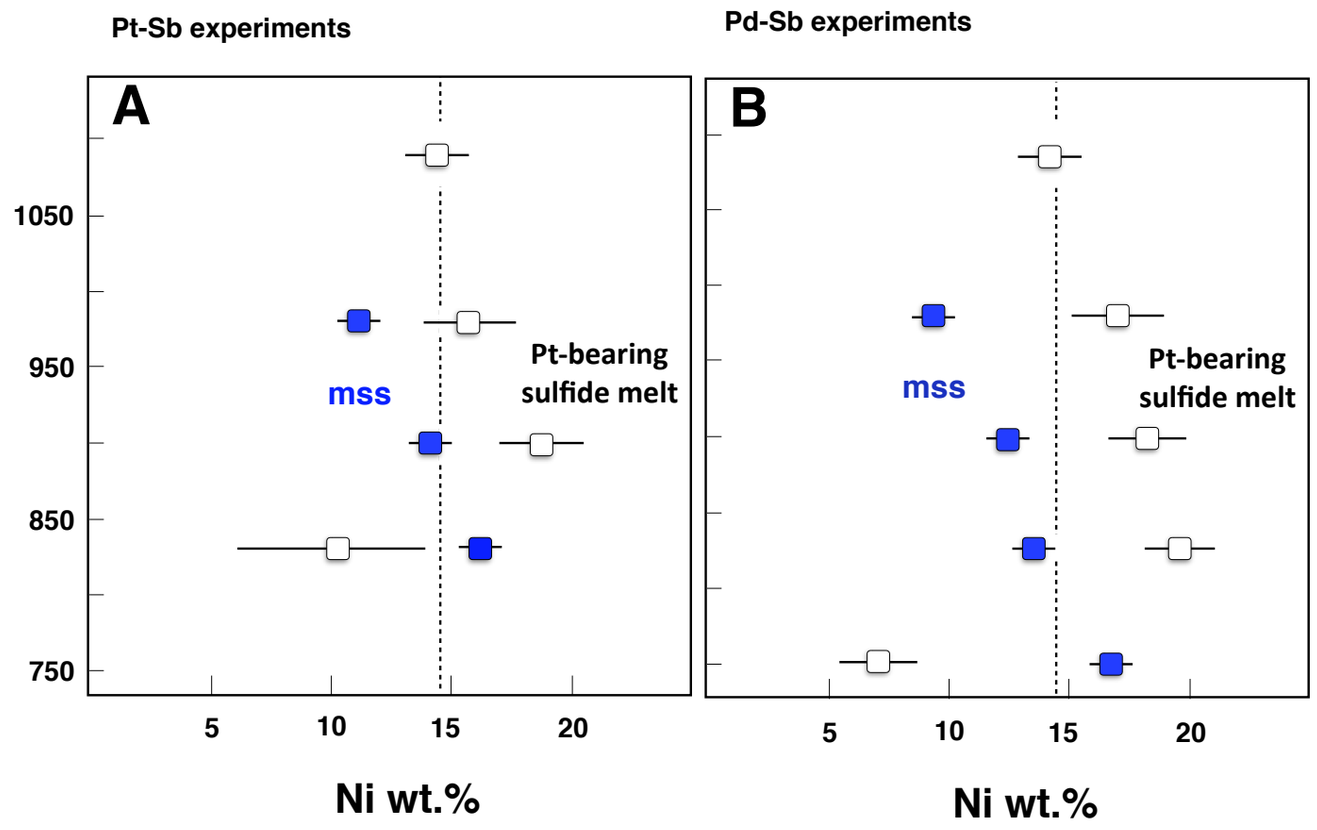

Figure 2

This is a preprint, the final version is subject to change, of the American Mineralogist (MSA)
Cite as Authors (Year) Title. American Mineralogist, in press.
DOI: https://doi.org/10.2138/am-2020-7154

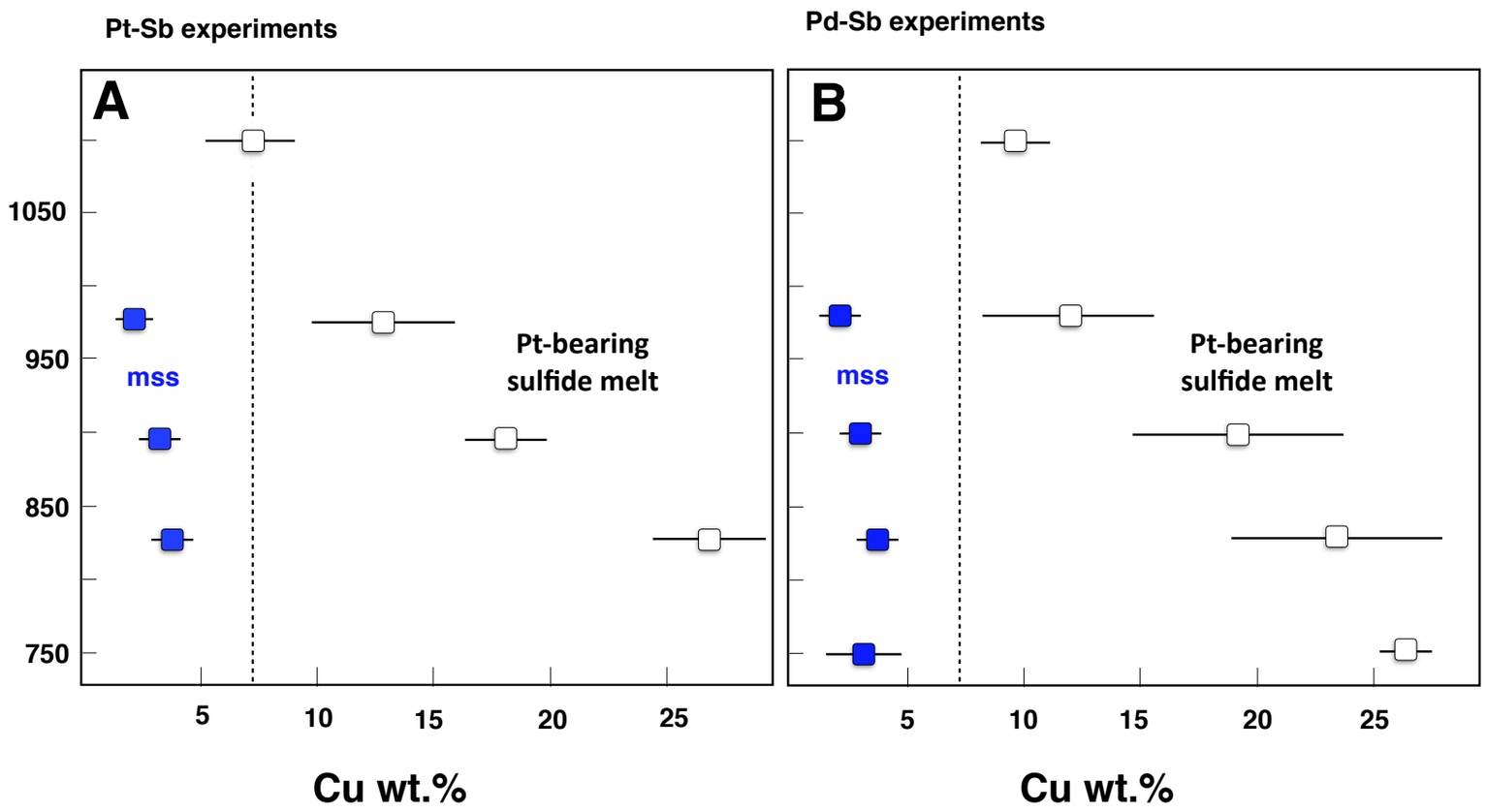

Figure 3

This is a preprint, the final version is subject to change, of the American Mineralogist (MSA)
Cite as Authors (Year) Title. American Mineralogist, in press.
DOI: https://doi.org/10.2138/am-2020-7154

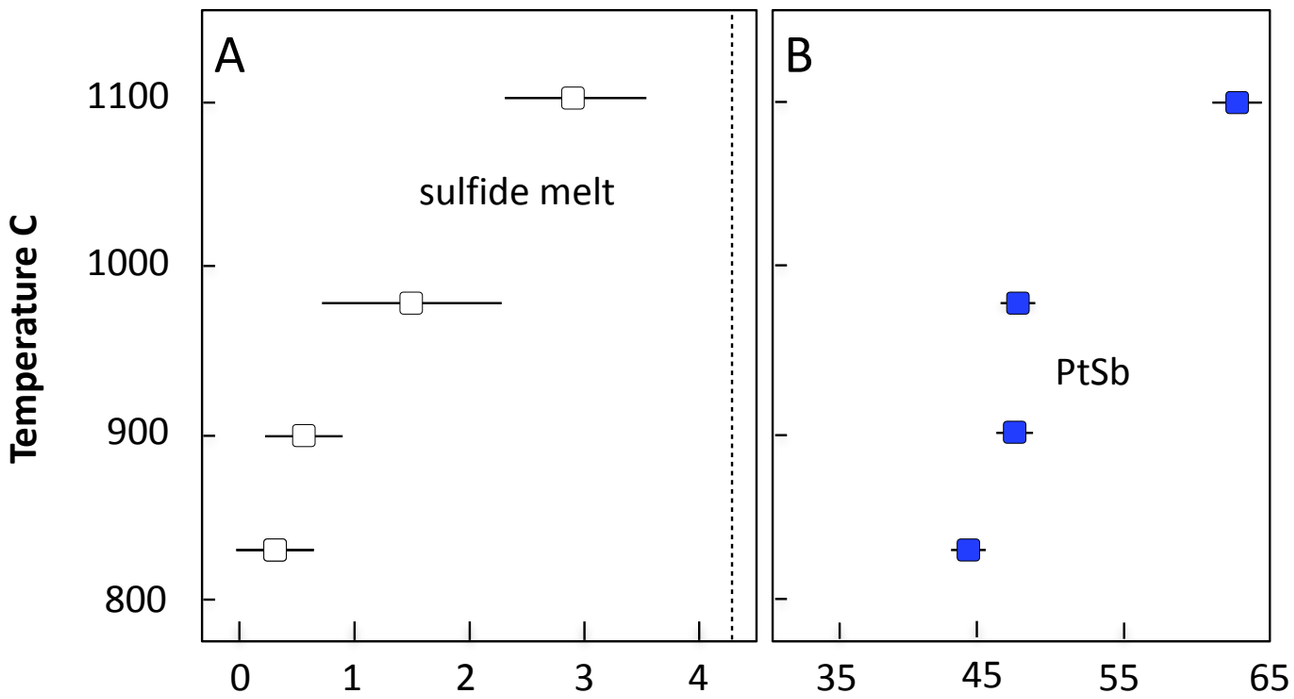

Figure 4

This is a preprint, the final version is subject to change, of the American Mineralogist (MSA)
Cite as Authors (Year) Title. American Mineralogist, in press.
DOI: https://doi.org/10.2138/am-2020-7154

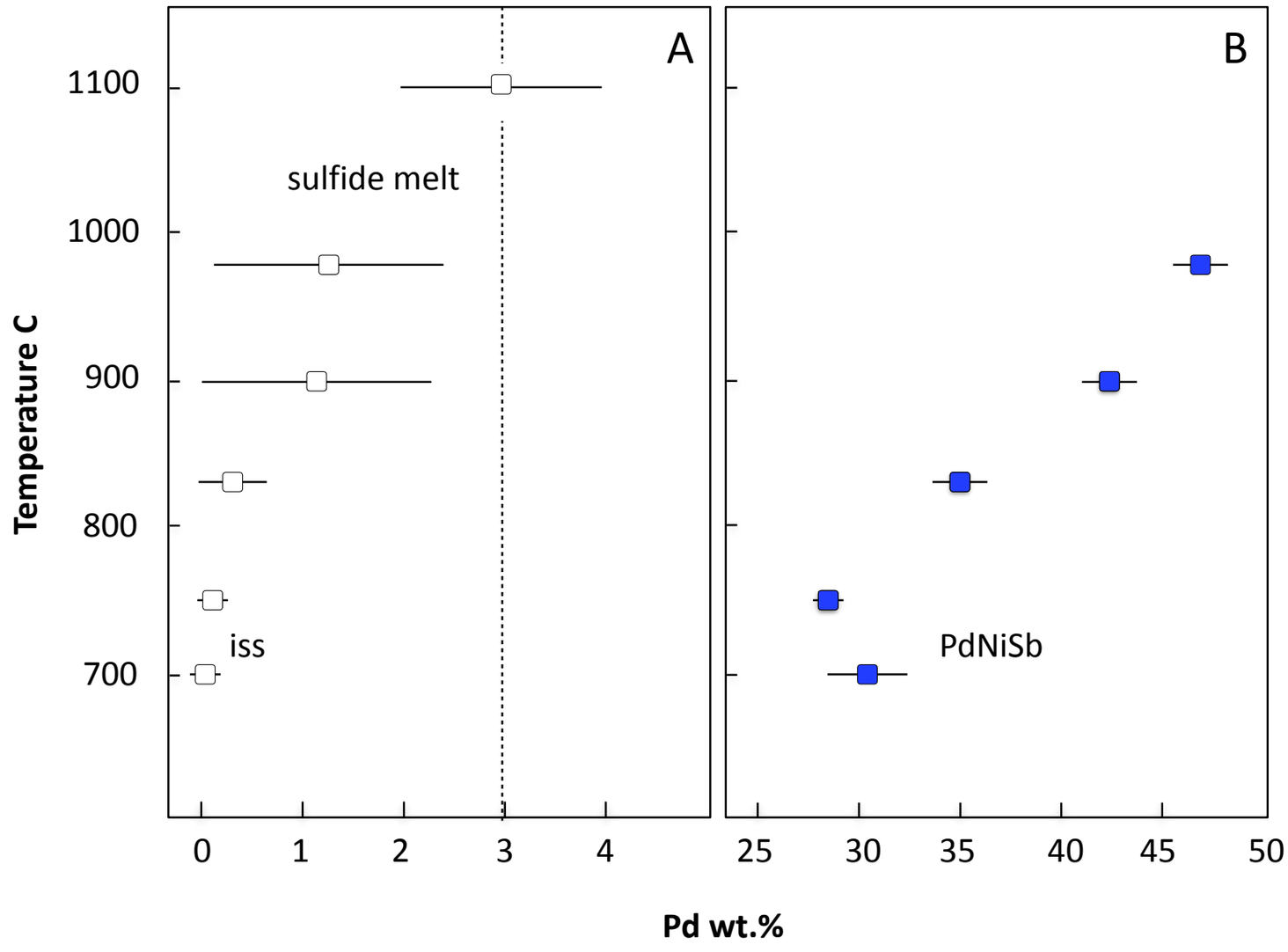

Figure 5

This is a preprint, the final version is subject to change, of the American Mineralogist (MSA)
Cite as Authors (Year) Title. American Mineralogist, in press.
DOI: https://doi.org/10.2138/am-2020-7154

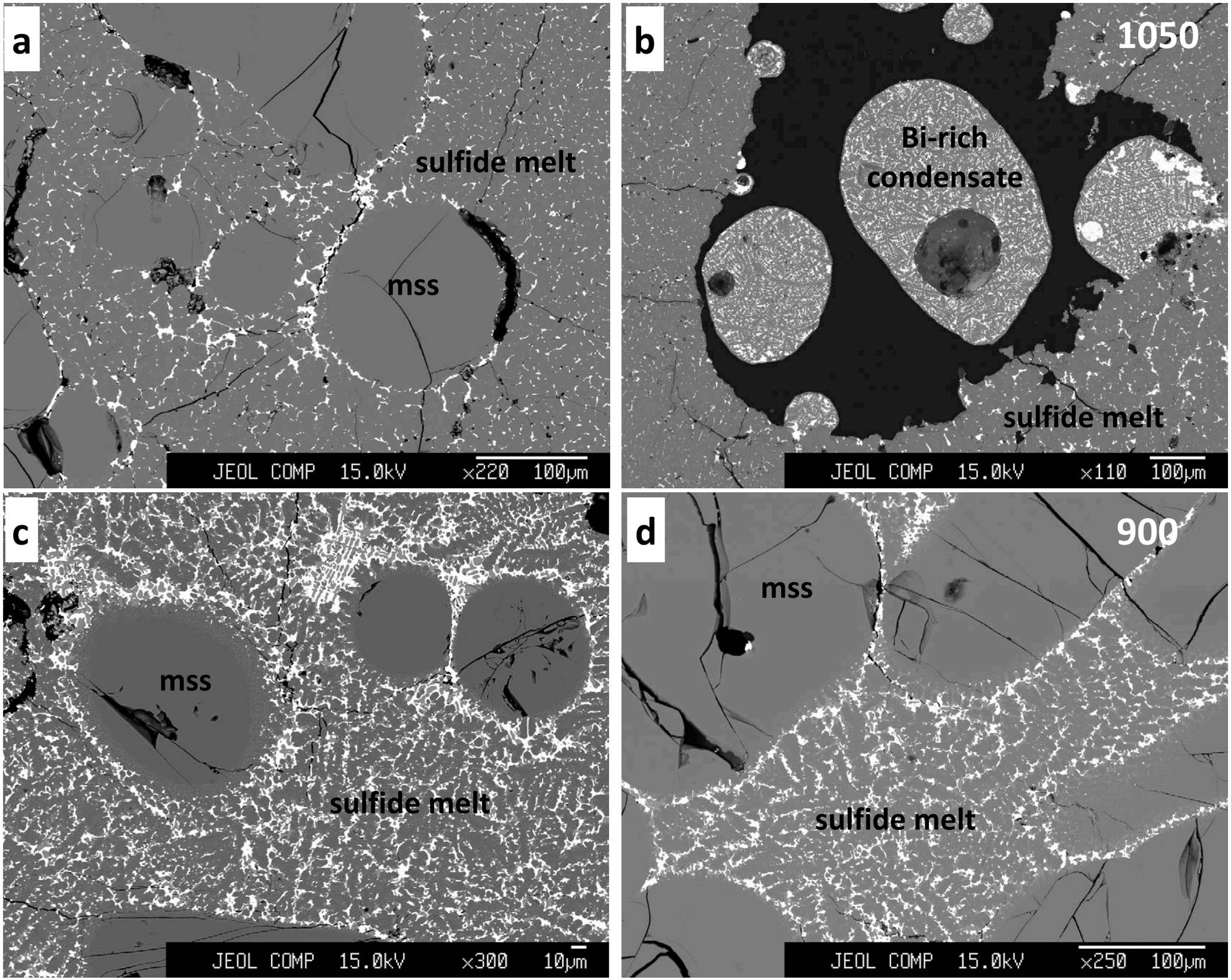

This is a preprint, the final version is subject to change, of the American Mineralogist (MSA)
Cite as Authors (Year) Title. American Mineralogist, in press.
DOI: https://doi.org/10.2138/am-2020-7154

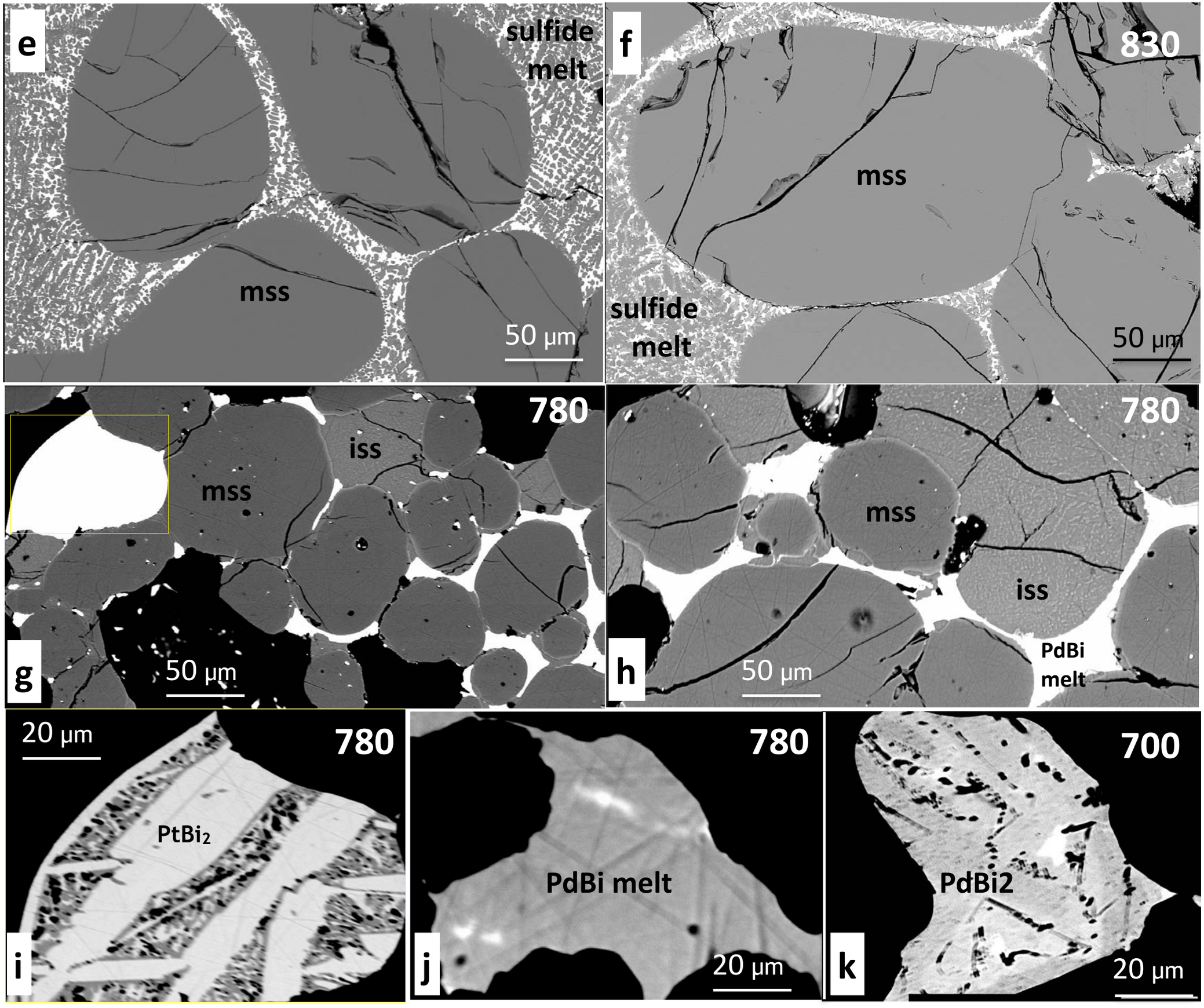

This is a preprint, the final version is subject to change, of the American Mineralogist (MSA)
Cite as Authors (Year) Title. American Mineralogist, in press.
DOI: https://doi.org/10.2138/am-2020-7154

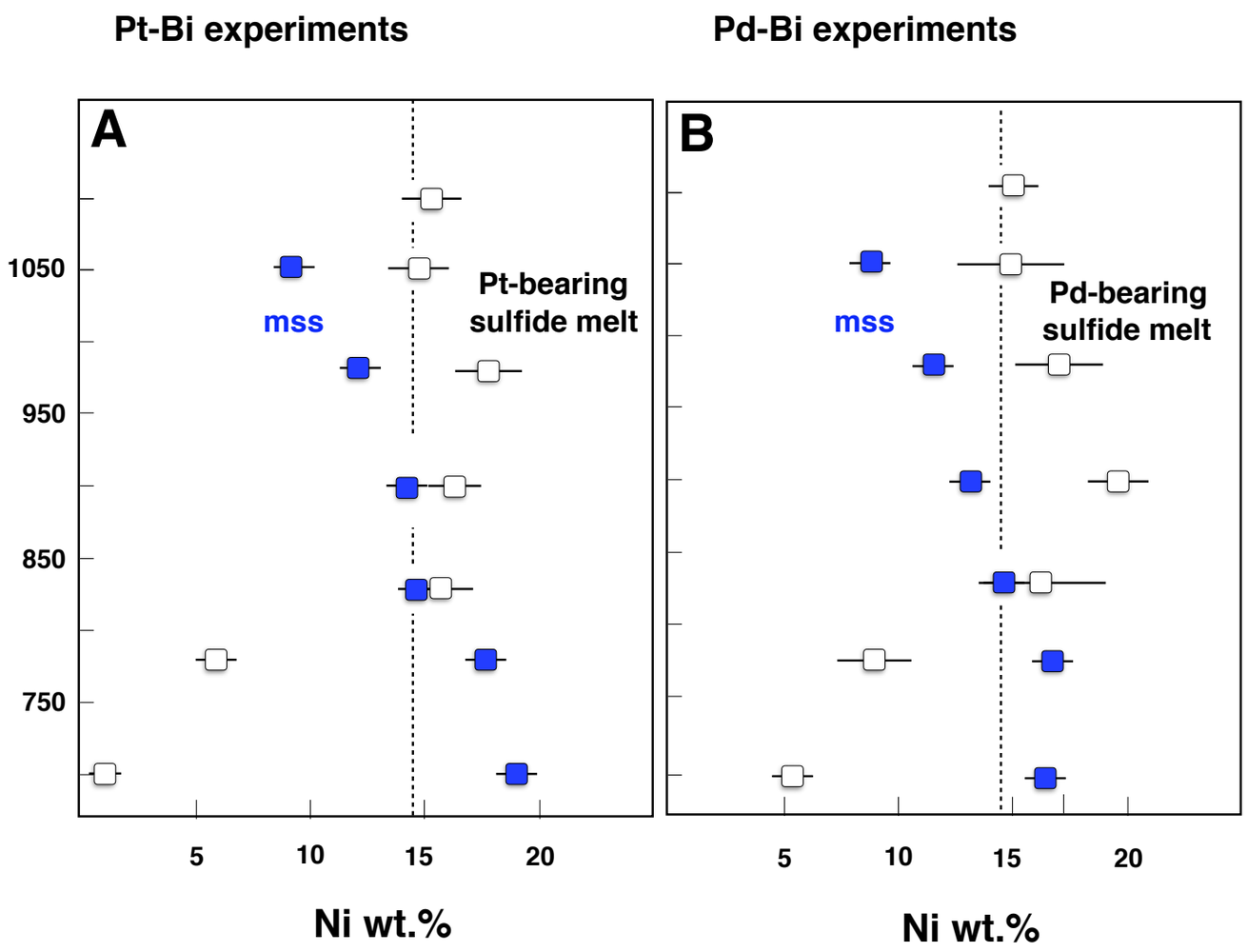

Figure 7

This is a preprint, the final version is subject to change, of the American Mineralogist (MSA)
Cite as Authors (Year) Title. American Mineralogist, in press.
DOI: https://doi.org/10.2138/am-2020-7154

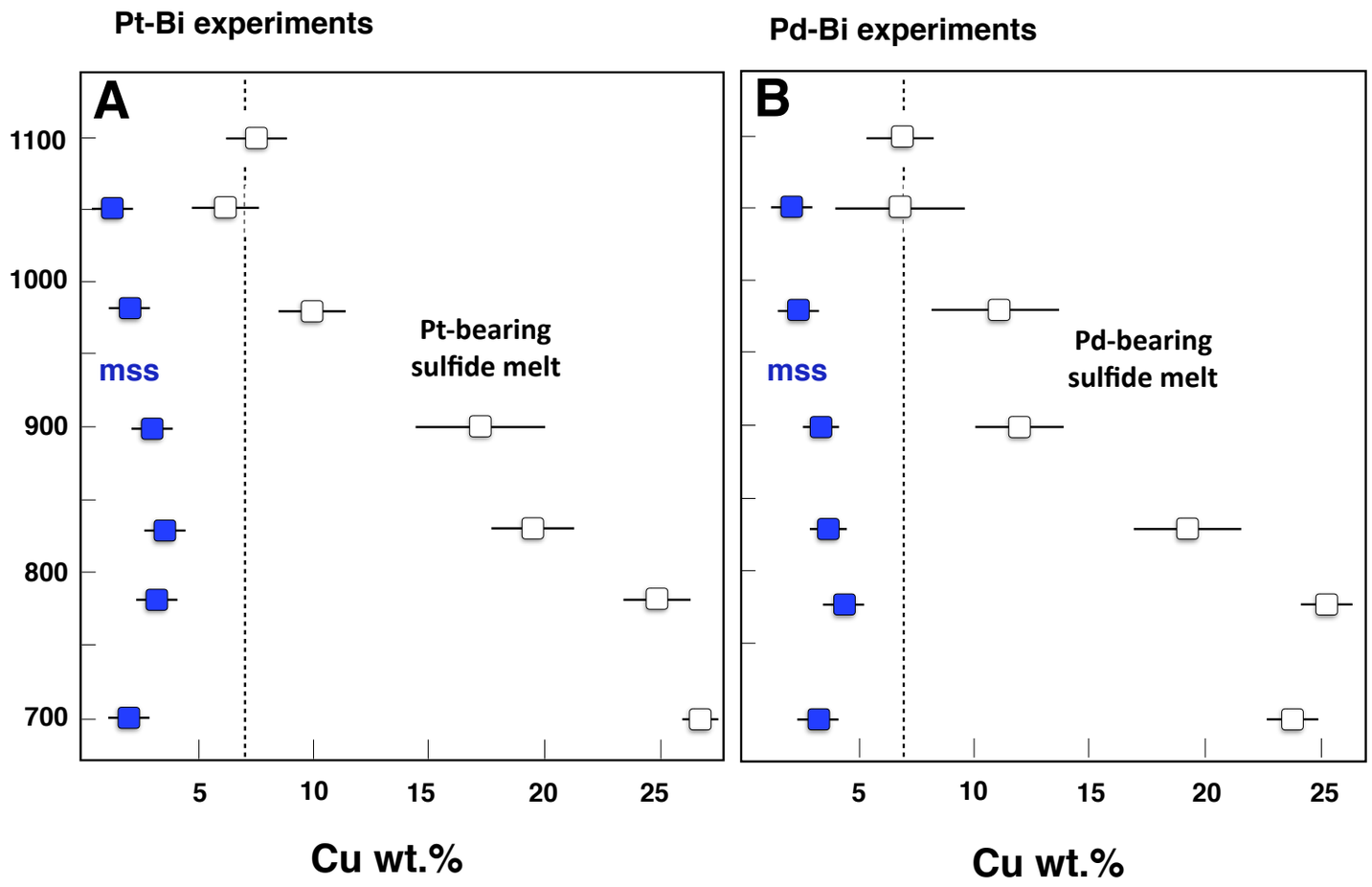

Figure 8

This is a preprint, the final version is subject to change, of the American Mineralogist (MSA)
Cite as Authors (Year) Title. American Mineralogist, in press.
DOI: https://doi.org/10.2138/am-2020-7154

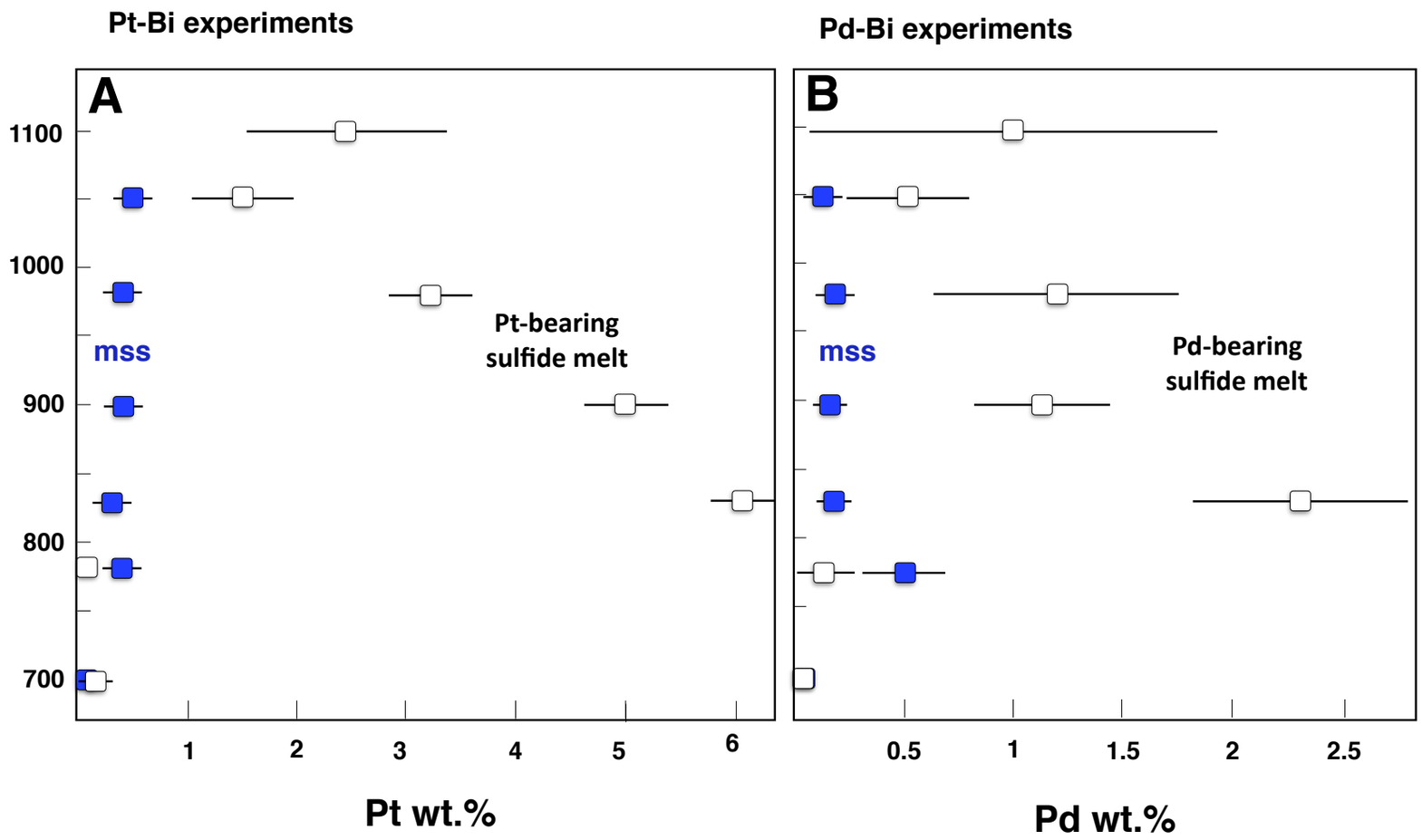

Figure 9

This is a preprint, the final version is subject to change, of the American Mineralogist (MSA)
Cite as Authors (Year) Title. American Mineralogist, in press.
DOI: https://doi.org/10.2138/am-2020-7154

Table 1. Starting sulfide, antimonide and bismuthinide compositions

	Sulfide matri	Antimonide components		Bismuthinide components	
Weight %		PdSb2	PtSb2	PdBi2	PtBi2
Fe	40.2				
Ni	16				
Cu	7.8				
Pd		30		20	
Pt			43.8		31.6
Sb		70	56.2		
Bi				80	68.4
S	36				

This is a preprint, the final version is subject to change, of the American Mineralogist (MSA)
Cite as Authors (Year) Title. American Mineralogist, in press.
DOI: https://doi.org/10.2138/am-2020-7154

Table 2. Summary of experimental conditions and run products

Run Number	Run T	Run time (h)	Run products
The antimonide system			
The Pd-Sb-sulfide system			
DS1	1100	12	supeliqudus
DS2	980	24	mss + sulfide melt + antimonide melt
DS3	900	48	mss + sulfide melt + antimonide melt
DS4	830	96	mss + sulfide melt + antimonide melt
DS5	750	120	mss + iss + nickeliferous sudburyite
The Pt-Sb-sulfide system			
TS1	1100	12	sulfide melt + antimonide melt
TS2	980	24	mss + geversite + sulfide melt
TS3	900	48	mss + geversite + sulfide melt
TS4	830	96	mss + geversite + iss
The bismuthinide system			
The Pd-Bi-sulfide system			
DI1	1100	12	supeliqudus
DB1	1050	24	mss + sulfide melt and bismuthinide melt?
DB2	980	24	mss + sulfide melt
DB3	900	48	mss + sulfide melt
DB4	830	96	mss + sulfide melt
DB5	780	120	mss + iss + bismuthinide melt
DB6	700	144	mss + iss + froodite
The Pt-Bi-sulfide system			
DI1	1100	12	supeliqudus
DB1	1050	24	mss + sulfide melt and bismuthinide melt?
DB2	980	24	mss + sulfide melt
DB3	900	48	mss + sulfide melt
DB4	830	96	mss + sulfide melt
DB5	780	120	mss + iss + Insizwaite + bismuthinide melt

This is a preprint, the final version is subject to change, of the American Mineralogist (MSA)
Cite as Authors (Year) Title. American Mineralogist, in press.
DOI: https://doi.org/10.2138/am-2020-7154

Table 3. Phase composition of the Pt-Sb-sulfide system

Phase	Antimonides				Sulfide phases		
	Sb melt	Geversite			Sulfide melt		
Run T(°C)	1100	980	900	830	1100	980	900
wt.%	n=5	n=5	n=5	n=4	n=5	n=5	n=5
Fe	0.10 ±0.03	0.20 ±0.06	0.51 ±0.38	0.71 ±0.20	38.81 ±1.42	33.71 ±2.97	30.08 ±0.97
Cu	1.02 ±0.25	0.05 ±0.05	0.22 ±0.15	0.30 ±0.06	6.90 ±1.81	12.74 ±3.39	17.63 ±2.49
Ni	1.75 ±0.19	0.06 ±0.06	0.25 ±0.11	0.24 ±0.07	13.99 ±0.61	15.51 ±1.76	18.53 ±1.44
Pt	60.12 ±1.10	45.01 ±0.61	44.83 ±0.29	41.42 ±0.64	2.90 ±0.63	1.47 ±0.84	0.54 ±0.29
Sb	37.00 ±0.65	54.70 ±0.12	55.23 ±0.24	53.80 ±0.30	3.77 ±0.81	3.12 ±0.52	1.79 ±0.80
S	0.32 ±0.13	0.17 ±0.03	0.06 ±0.05	b.d.l	33.04 ±0.86	32.41 ±1.67	31.81 ±0.74
Total	100.30	100.19	101.10	96.49	99.41	98.97	100.38
Atomic proportions							
Fe	0.003 ±0.001	0.005 ±0.002	0.013 ±0.009	0.019 ±0.005	0.328 ±0.007	0.285 ±0.018	0.251 ±0.006
Cu	0.024 ±0.006	0.001 ±0.001	0.005 ±0.003	0.007 ±0.001	0.051 ±0.014	0.095 ±0.027	0.130 ±0.021
Ni	0.045 ±0.005	0.002 ±0.001	0.006 ±0.003	0.006 ±0.002	0.113 ±0.003	0.125 ±0.014	0.147 ±0.012
Pt	0.460 ±0.011	0.334 ±0.004	0.327 ±0.006	0.314 ±0.004	0.007 ±0.002	0.004 ±0.002	0.001 ±0.001
Sb	0.453 ±0.007	0.651 ±0.005	0.646 ±0.007	0.653 ±0.003	0.015 ±0.003	0.012 ±0.002	0.007 ±0.003
S	0.015 ±0.006	0.007 ±0.001	0.003 ±0.002	0.001 ±0.001	0.486 ±0.005	0.478 ±0.012	0.463 ±0.006

This is a preprint, the final version is subject to change, of the American Mineralogist (MSA)
Cite as Authors (Year) Title. American Mineralogist, in press.
DOI: https://doi.org/10.2138/am-2020-7154

Monosulfide solid solution			
830	980	900	830
n=5	n=5	n=6	n=5
29.24 ±6.25	49.61 ±0.10	45.82 ±0.40	44.23 ±0.72
27.55 ±4.19	2.33 ±0.10	2.94 ±0.21	3.49 ±0.20
10.08 ±5.17	10.95 ±0.10	14.46 ±0.14	16.05 ±0.24
0.09 ±0.15	0.13 ±0.12	0.30 ±0.23	b.d.l
2.17 ±1.78	b.d.l	b.d.l	b.d.l
32.52 ±1.80	37.18 ±0.17	37.00 ±0.27	37.71 ±0.29
101.67	100.19	######	101.68
0.241 ±0.045	0.391 ±0.001	0.362 ±0.002	0.34 ±0.006
0.201 ±0.035	0.016 ±0.001	0.020 ±0.002	0.02 ±0.001
0.08 ±0.041	0.082 ±0.001	0.109 ±0.001	0.12 ±0.002
2E-04	0.000	0.001 ±0.001	0.00
0.008 ±0.007			
0.469 ±0.013	0.510 ±0.001	0.509 ±0.003	0.51 ±0.004

This is a preprint, the final version is subject to change, of the American Mineralogist (MSA)
Cite as Authors (Year) Title. American Mineralogist, in press.
DOI: https://doi.org/10.2138/am-2020-7154

Table 4. Phase composition of the Pd-Sb sulfide system

Phase	Antimonides				Sulfide phases				
	Sb melt			Sudburyite	Sulfide melt				ISS
Run T(°C)	980	900	830	750	1100	980	900	830	750
	n=7	n=5	n=5	n=5	n=6	n=6	n=5	n=5	n=5
Fe	0.09 ±0.10	0.05 ±0.07	0.09 ±0.08	0.24 ±0.19	36.55 ±1.37	31.74 ±2.91	22.21 ±2.46	21.37 ±1.65	32.25
Cu	0.92 ±0.37	1.15 ±0.14	1.84 ±0.15	0.43 ±0.14	9.72 ±1.85	11.93 ±4.17	19.33 ±4.98	23.54 ±5.21	26.68
Ni	1.83 ±0.47	3.31 ±0.41	7.43 ±0.67	11.70 ±0.07	14.29 ±0.83	16.82 ±2.27	17.97 ±3.71	19.57 ±3.22	5.67
Pd	46.62 ±1.16	42.23 ±1.10	34.56 ±0.95	28.26 ±0.09	2.94 ±0.92	1.22 ±1.18	1.13 ±1.22	0.30 ±0.30	0.04
Sb	49.63 ±0.47	52.42 ±0.33	54.39 ±0.43	58.61 ±0.19	4.46 ±1.60	6.00 ±1.95	12.14 ±3.35	8.00 ±3.45	0.17
S	0.33 ±0.06	0.41 ±0.11	1.16 ±0.17	0.02 ±0.02	33.19 ±1.14	32.28 ±1.43	28.09 ±2.21	28.40 ±1.42	33.06
Total	99.42	99.58	#####	99.26	#####	99.99	#####	#####	97.87
Fe	0.002 ±0.002	0.001 ±0.001	0.002 ±0.002	0.004 ±0.004	0.306 ±0.007	0.269 ±0.020	0.199 ±0.017	0.187 ±0.011	0.271
Cu	0.016 ±0.006	0.020 ±0.002	0.030 ±0.002	0.007 ±0.002	0.072 ±0.014	0.089 ±0.032	0.153 ±0.042	0.182 ±0.040	0.197
Ni	0.034 ±0.009	0.061 ±0.007	0.131 ±0.010	0.208 ±0.001	0.114 ±0.006	0.136 ±0.016	0.153 ±0.029	0.163 ±0.026	0.045
Pd	0.483 ±0.015	0.432 ±0.012	0.336 ±0.013	0.277 ±0.002	0.008 ±0.004	0.005 ±0.005	0.005 ±0.006	0.001 ±0.002	0.000
Sb	0.450 ±0.003	0.469 ±0.003	0.462 ±0.003	0.502 ±0.004	0.017 ±0.007	0.023 ±0.008	0.050 ±0.015	0.032 ±0.015	0.001
S	0.011 ±0.002	0.014 ±0.004	0.037 ±0.005	0.001	0.484 ±0.009	0.477 ±0.010	0.439 ±0.021	0.434 ±0.012	0.485

This is a preprint, the final version is subject to change, of the American Mineralogist (MSA)
Cite as Authors (Year) Title. American Mineralogist, in press.
DOI: https://doi.org/10.2138/am-2020-7154

	Monosulfide solid solution							
	980		900		830		750	
	n=5		n=5		n=5		n=5	
±0.48	51.54	±0.26	48.52	±0.21	48.32	±0.36	42.62	±0.28
±0.49	2.04	±0.03	2.73	±0.18	3.31	±0.16	2.73	±1.41
±0.28	9.16	±0.08	12.22	±0.18	13.44	±0.10	16.65	±1.75
±0.09	0.09	±0.04	0.02	±0.01	0.00	±0.01	0.01	±0.01
±0.14	b.d.l		b.d.l		b.d.l		b.d.l	
±0.16	37.25	±0.29	37.06	±0.17	37.64	±0.30	37.09	±0.69
	#####		#####		#####		99.13	
±0.003	0.406	±0.001	0.382	±0.002	0.373	±0.003	0.340	±0.005
±0.004	0.014		0.019		0.022	±0.001	0.019	±0.010
±0.002	0.069	±0.001	0.091	±0.001	0.099	±0.001	0.126	±0.012
±0.001	0.000		0.000		0.000		0.000	
±0.001								
±0.002	0.511	±0.001	0.508	±0.001	0.506	±0.003	0.515	±0.004

This is a preprint, the final version is subject to change, of the American Mineralogist (MSA)
Cite as Authors (Year) Title. American Mineralogist, in press.
DOI: https://doi.org/10.2138/am-2020-7154

Table 5. Phase composition of the Pt-Bi sulfide system

Phase	Bismuthinides				Sulfide phases																	
					Sulfide melt and iss																	Monosu
Run T(°C)	780		700		1100		1050		980		900		830		780		700					1050
	n=4		n=5		n=6		n=5		n=7		n=5		n=5		n=4		n=4					n=8
Fe	0.06	±0.05	1.19	±0.23	38.37	±1.69	39.76	±3.39	31.66	±3.05	23.29	±1.67	17.75	±2.13	34.78	±0.52	33.77	±0.50				52.06
Cu	0	0	0.00	0	7.24	±0.96	6.10	±1.28	9.982	±1.29	17.24	±2.80	19.48	±1.84	25.08	±0.79	26.87	±0.98				1.35
Ni	0.03	±0.01	0.56	±0.16	15.38	±1.17	14.65	±1.08	17.51	±1.23	15.98	±1.29	15.51	±1.37	5.88	±0.79	6.02	±0.28				9.24
Pt	33.84	±0.41	32.31	±1.35	2.44	±1.29	1.48	±0.72	3.244	±0.62	5.02	±0.78	5.96	±0.81	0.01	±0.01	0.23	±0.05				0.45
Bi	66.15	±0.32	66.96	±1.26	3.88	±2.16	4.46	±3.72	6.532	±2.55	11.52	±3.32	15.42	±3.94	0.17	±0.02	0.47	±0.85				0.20
S	0.17	±0.01	0.12	±0.03	33.98	±1.33	34.41	±2.26	32.66	±1.66	28.56	±1.60	27.06	±1.86	31.63	±0.33	31.84	±0.62				37.98
Total	100.25		101.13		101.29		100.86		101.59		101.61		101.20		97.54		99.20					101.28
Fe	0.002	0.003	0.041	0.007	0.319	±0.008	0.344	±0.013	0.271	±0.015	0.230	±0.010	0.184	±0.014	0.296	0.004	0.284	0.004				0.416
Cu					0.053	±0.009	0.044	±0.011	0.075	±0.013	0.141	±0.024	0.167	±0.017	0.187	0.006	0.199	0.007				0.009
Ni	0.001	0.001	0.018	0.005	0.122	±0.004	0.078	±0.004	0.143	±0.013	0.091	±0.013	0.099	±0.005	0.048	0.012	0.048	0.007				0.046
Pt	0.349	0.006	0.318	0.013	0.005	±0.006	0.004	±0.004	0.008	±0.004	0.014	±0.005	0.018	±0.005	1E-05	7E-04	0.001	7E-04				0.001
Bi	0.637	0.007	0.616	0.015	0.009	±0.007	0.011	±0.010	0.015	±0.008	0.031	±0.010	0.043	±0.013	0.000		0.001	0.007				
S	0.011	0.001	0.007	0.001	0.493	±0.006	0.519	±0.009	0.488	±0.013	0.492	±0.013	0.488	±0.011	0.469	0.005	0.467	0.009				0.528

This is a preprint, the final version is subject to change, of the American Mineralogist (MSA)
Cite as Authors (Year) Title. American Mineralogist, in press.
DOI: https://doi.org/10.2138/am-2020-7154

ılfide solid solution

980		900		830		780		700	
n=6		n=5		n=7		n=5		n=4	
±0.32	49.36 ±1.18	45.81 ±0.72		45.55 ±0.59		42.65 ±0.24		41.91 ±0.31	
±0.09	2.075 ±0.21	2.69 ±0.09		3.28 ±0.14		2.92 ±0.54		2.23 ±0.21	
±0.47	11.61 ±0.26	13.74 ±0.42		14.70 ±0.37		17.39 ±0.22		18.72 ±0.13	
±0.31	0.296 ±0.17	0.32 ±0.11		0.21 ±0.14		0.32 ±0.34		0 ±0.01	
±0.07	0.217 ±0.11	0.20 ±0.10		0.21 ±0.11		0.19 ±0.06		0.19 ±0.11	
±0.34	37.71 ±0.32	37.06 ±0.42		36.99 ±0.39		36.15 ±0.19		36.49 ±0.17	
	101.27	99.82		100.93		99.62		99.54	
±0.002	0.385 ±0.008	0.378 ±0.003		0.374 ±0.004		0.342	0.003	0.332	0.004
±0.001	0.014 ±0.001	0.018 ±0.001		0.022 ±0.001		0.021	0.001	0.017	0.001
±0.002	0.086 ±0.003	0.070 ±0.002		0.075 ±0.002		0.133	0.001	0.142	0.001
±0.001	0.001 ±0.001	0.001 ±0.001		0.000 ±0.001		7E-04	0.008	6E-04	6E-04
±0.003	0.513 ±0.005	0.533 ±0.003		0.528 ±0.004		0.504	0.002	0.507	0.002

This is a preprint, the final version is subject to change, of the American Mineralogist (MSA)
Cite as Authors (Year) Title. American Mineralogist, in press.
DOI: https://doi.org/10.2138/am-2020-7154

Table 6. Phase composition of the Pd-Bi sulfide system

Phase	Bismuthinides			Sulfides						
	Bi melt		Froodite	Sulfide melt						iss
Run T(°C)	1050	780	700	1100	1050	980	900	830	780	700
	n=5		n=5	n=6	n=7	n=6	n=5	n=6		n=7
Fe	16.57 ±2.86	0.70 ±0.24	0.57 ±0.43	41.48 ±1.37	39.83 ±2.55	30.75 ±3.95	27.43 ±1.55	19.60 ±2.31	33.39 ±0.57	37.24 ±0.37
Cu	20.51 ±1.54	0.34 ±0.08	0.09 ±0.07	6.52 ±0.88	6.46 ±3.01	10.86 ±2.97	11.78 ±1.91	19.13 ±2.82	25.22 ±0.45	23.60 ±0.31
Ni	14.13 ±1.78	0.42 ±0.06	0.26 ±0.21	15.00 ±0.65	14.86 ±2.09	17.00 ±1.78	19.66 ±1.41	16.18 ±2.47	8.80 ±1.44	5.11 ±0.34
Pd	2.41 ±0.69	19.35 ±0.29	15.75 ±1.00	1.11 ±0.93	0.52 ±0.42	1.23 ±0.71	1.12 ±0.43	2.31 ±0.79	0.16 ±0.23	0.02 ±0.02
Bi	20.65 ±6.96	78.01 ±0.66	81.47 ±0.49	4.20 ±1.17	4.14 ±2.55	8.29 ±4.16	7.97 ±2.27	15.64 ±4.11	0.15 ±0.03	0.10 ±0.05
S	25.66 ±2.64	0.05 ±0.02	0.18 ±0.17	33.09 ±1.03	34.65 ±1.30	32.05 ±1.87	31.72 ±1.21	27.78 ±2.16	31.65 ±0.36	34.68 ±0.31
Total	99.94 ±1.54	98.87 ±0.76	98.32 ±1.06	101.4	100.46 ±0.98	100.47 ±2.19	99.69 ±1.15	100.64 ±0.67	99.37 ±0.63	100.74 ±0.63
Fe	0.176 ±0.020	0.025 0.008	0.018 ±0.013	0.34 ±0.009	0.343 ±0.015	0.267 ±0.017	0.255 ±0.009	0.197 ±0.016	0.280 0.005	0.309 ±0.003
Cu	0.181 ±0.016	0.011 0.003	0.002 ±0.002	0.05 ±0.007	0.046 ±0.022	0.083 ±0.013	0.091 ±0.015	0.160 ±0.026	0.186 0.003	0.162 ±0.003
Ni	0.093 ±0.009	0.014 0.002	0.005 ±0.004	0.12 ±0.003	0.079 ±0.010	0.140 ±0.009	0.113 ±0.007	0.101 ±0.013	0.070 0.011	0.026 ±0.002
Pd	0.014 ±0.005	0.199 0.005	0.265 ±0.016	0.01 ±0.002	0.002 ±0.002	0.006 ±0.001	0.006 ±0.002	0.012 ±0.005	0.000 0.001	
Bi	0.060 ±0.025	0.748 0.004	0.699 ±0.012	0.01 ±0.003	0.010 ±0.006	0.019 ±0.010	0.020 ±0.006	0.043 ±0.013	0.000 0.000	
S	0.476 ±0.018	0.003 0.001	0.010 ±0.010	0.48 ±0.007	0.520 ±0.007	0.485 ±0.011	0.515 ±0.008	0.488 ±0.016	0.463 0.006	0.502 ±0.002

This is a preprint, the final version is subject to change, of the American Mineralogist (MSA)
Cite as Authors (Year) Title. American Mineralogist, in press.
DOI: https://doi.org/10.2138/am-2020-7154

Monosulfide solid solution					
1050	980	900	830	780	700
n=5	n=5	n=5	n=5		n=5
52.17 ±1.49	49.53 ±0.41	46.80 ±0.59	46.09 ±0.57	40.10 ±0.21	43.62 ±0.41
1.72 ±0.39	**1.81** ±0.09	2.64 ±0.09	3.04 ±0.10	3.83 ±0.29	2.70 ±0.21
8.88 ±0.31	11.37 ±0.61	13.15 ±0.38	14.43 ±0.43	17.29 ±0.19	16.51 ±0.44
0.09 ±0.06	0.177 ±0.06	0.13 ±0.04	0.14 ±0.06	0.52 ±0.36	0.08 ±0.03
0.21 ±0.13	**0.154** ±0.10	0.21 ±0.06	0.23 ±0.06	0.20 ±0.04	0.15 ±0.10
37.40 ±0.48	37.65 ±0.69	37.00 ±0.47	37.07 ±0.71	37.44 ±0.25	37.25 ±0.35
100.46 ±1.35	100.9 ±1.15	99.93 ±0.94	100.99 ±1.29	99.38 ±0.75	100.31 ±0.56
0.419 ±0.006	0.388 ±0.003	0.384 ±0.001	0.377 ±0.003	0.329 0.001	0.360 ±0.003
0.011 ±0.003	0.012 ±0.001	0.018 ±0.001	0.021 ±0.001	0.028 0.002	0.018 ±0.001
0.044 ±0.002	0.085 ±0.002	0.067 ±0.002	0.073 ±0.002	0.135 0.002	0.084 ±0.002
	0.001	0.001	0.001 ±0.000	0.001 0.001	
	0.000	0.000		0.000 0.000	
0.524 ±0.002	0.514 ±0.004	0.529 ±0.003	0.528 ±0.004	0.507 0.002	0.536 ±0.003